J. Space Weather Space Clim., **6**, A39 (2016)
DOI: 10.1051/swsc/2016034

RESEARCH ARTICLE OPEN ACCESS

DOSIS & DOSIS 3D: long-term dose monitoring onboard the Columbus Laboratory of the International Space Station (ISS)

Thomas Berger*[,1], Bartos Przybyla[1], Daniel Matthiä[1], Günther Reitz[1], Sönke Burmeister[2], Johannes Labrenz[2], Pawel Bilski[3], Tomasz Horwacik[3], Anna Twardak[3], Michael Hajek[4,5], Manfred Fugger[5], Christina Hofstätter[5], Lembit Sihver[5,6], Jozsef K. Palfalvi[7], Julianna Szabo[7], Andrea Stradi[7], Iva Ambrozova[8], Jan Kubancak[8], Katerina Pachnerova Brabcova[8], Filip Vanhavere[9], Vanessa Cauwels[9], Olivier Van Hoey[9], Werner Schoonjans[9], Alessio Parisi[9], Ramona Gaza[10,11], Edward Semones[10], Eduardo G. Yukihara[12], Eric R. Benton[12], Brandon A. Doull[12], Yukio Uchihori[13], Satoshi Kodaira[13], Hisashi Kitamura[13], and Matthias Boehme[14]

[1] German Aerospace Center (DLR), Institute of Aerospace Medicine, Linder Höhe, 51147 Köln, Germany
*Corresponding author: thomas.berger@dlr.de
[2] Christian Albrechts Universität zu Kiel (CAU), Christian-Albrechts-Platz, 24118 Kiel, Germany
[3] Institute of Nuclear Physics, Polish Academy of Sciences (IFJ), PL-31342 Krakow, Poland
[4] International Atomic Energy Agency (IAEA), Division of Radiation, Transport and Waste Safety, 1400 Vienna, Austria
[5] Technische Universität Wien, Atominstitut (ATI), Stadionallee 2, 1020 Vienna, Austria
[6] EGB MedAustron, Marie-Curie-Straße 5, 2700 Wiener Neustadt, Austria
[7] Centre for Energy Research, (MTA EK), Konkoly Thege ut 29-33, 1121 Budapest, Hungary
[8] Nuclear Physics Institute of the CAS (NPI), Department of Radiation Dosimetry, Na Truhlarce 39/64, 180 00 Prague, Czech Republic
[9] Belgian Nuclear Research Center (SCK·CEN), Boeretang 200, 2400 Mol, Belgium
[10] NASA, Space Radiation Analysis Group (NASA/SRAG), Houston, TX 77058, USA
[11] Leidos, Exploration & Mission Support, 2400 NASA Pkwy, Houston, TX 77058, USA
[12] Physics Department, Oklahoma State University (OSU), Stillwater, OK 74078, USA
[13] National Institute of Radiological Sciences (NIRS), National Institutes for Quantum and Radiological Science and Technology (QST), 4-9-1 Anagawa, Inage, 263-8555 Chiba, Japan
[14] OHB System AG, Universitätsallee 27-29, 28359 Bremen, Germany

Received 26 July 2016 / Accepted 19 September 2016

ABSTRACT

The radiation environment encountered in space differs in nature from that on Earth, consisting mostly of highly energetic ions from protons up to iron, resulting in radiation levels far exceeding the ones present on Earth for occupational radiation workers. Since the beginning of the space era, the radiation exposure during space missions has been monitored with various active and passive radiation instruments. Also onboard the International Space Station (ISS), a number of area monitoring devices provide data related to the spatial and temporal variation of the radiation field in and outside the ISS. The aim of the DOSIS (2009–2011) and the DOSIS 3D (2012–ongoing) experiments was and is to measure the radiation environment within the European Columbus Laboratory of the ISS. These measurements are, on the one hand, performed with passive radiation detectors mounted at 11 locations within Columbus for the determination of the spatial distribution of the radiation field parameters and, on the other, with two active radiation detectors mounted at a fixed position inside Columbus for the determination of the temporal variation of the radiation field parameters. Data measured with passive radiation detectors showed that the absorbed dose values inside the Columbus Laboratory follow a pattern, based on the local shielding configuration of the radiation detectors, with minimum dose values observed in the year 2010 of 195–270 μGy/day and maximum values observed in the year 2012 with values ranging from 260 to 360 μGy/day. The absorbed dose is modulated by (a) the variation in solar activity and (b) the changes in ISS altitude.

Key words. International Space Station – Columbus – Space radiation – DOSIS – DOSIS 3D

1. Introduction

It is well known that the radiation field in free space is one of the most complex natural radiation fields consisting of contributions from Galactic Cosmic Rays (GCR) and protons due to sporadic Solar Particle Events (SPE) (Nelson 2016). These two sources contribute to the radiation load as, for example, on the way to Mars and can lead to dose equivalent values only from GCR exposure of up to 1.84 mSv/day (Zeitlin et al. 2013). In Low Earth Orbit (LEO), a third contribution to human radiation exposure is given by the trapped particles in the Earth radiation belts (Van Allen belts), particularly when the International Space Station (ISS) crosses the South Atlantic Anomaly (SAA) (Reitz 2008). Further on, the radiation field inside the ISS is modulated due to different local shielding thicknesses as well as due to orbital changes of the ISS. Determination of radiation environmental parameters is essentially aimed at gaining knowledge about the internal radiation

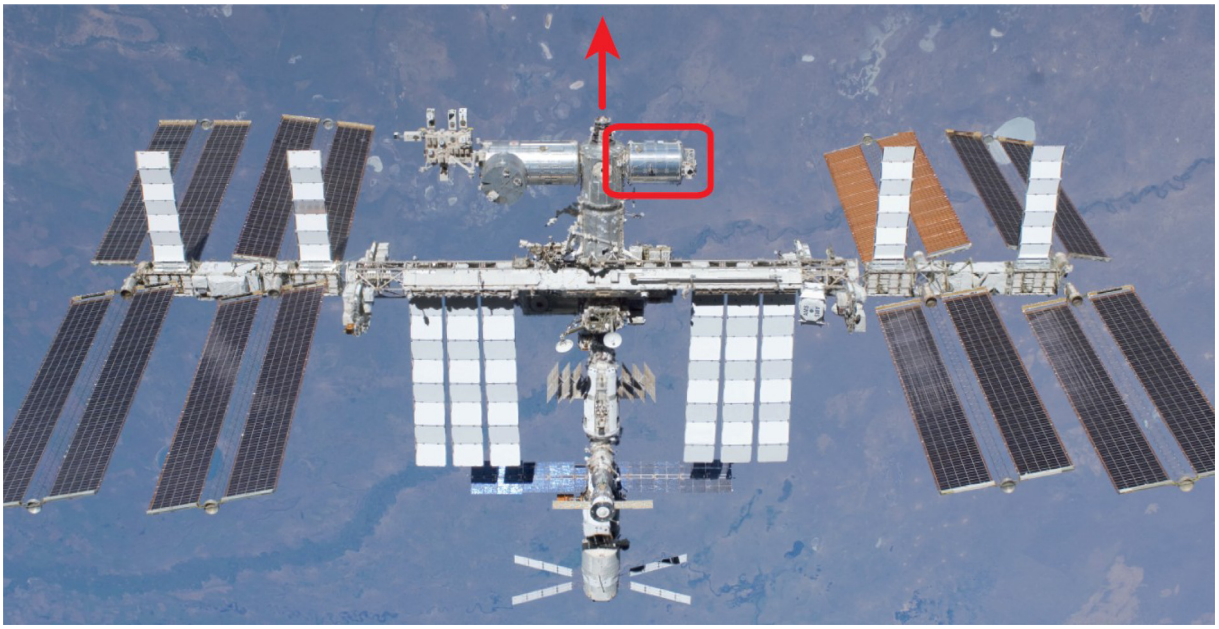

Fig. 1. The International Space Station (ISS) (picture taken by an STS-134 crew member on the space shuttle Endeavor, May 29, 2011) with the European Columbus Laboratory (in red) and the ISS flight direction (red arrow) Source: NASA.

environment onboard the ISS. In addition; only a reliably measured dataset for radiation exposure and the variation of the radiation load enables us to (a) use this data as input for radiation model and benchmark calculations (Matthiä et al. 2016) and (b) work toward a reasonably good radiation risk estimation for future long duration space missions (Durante & Cucinotta 2011). The radiation environment onboard the ISS has been monitored since the beginning of the ISS era with various active and passive radiation detector systems (see reviews in: Berger 2008; Caffrey & Hamby 2011; Narici et al. 2015) aiming for exact area monitoring within (Kodaira et al. 2014) and outside the ISS (Berger et al. 2015). Furthermore; various experiments aimed at determining the effective dose equivalent using phantoms for the improvement of radiation risk estimations have been performed (see for example: Reitz et al. 2009; Berger et al. 2013, Puchalska et al. 2014). In addition, passive radiation detector systems have been used as operational personal radiation detectors of the astro- and cosmonauts (Straube et al. 2010). The DOSIS and DOSIS 3D experiments currently performed onboard the ISS are aimed at improving our understanding of the radiation environment onboard the ISS and providing a set of data that can be used by the radiation research community for the benchmarking of radiation transport codes, as well for providing input to build a real 3D model of the radiation environment inside the ISS.

2. The DOSIS and DOSIS 3D experiments

The aim of the DOSIS (2009–2011) and the DOSIS 3D (2012–ongoing) experiments was and is to measure the radiation environment within the European Columbus Laboratory of the ISS (see Fig. 1).

These measurements are, on the one hand, performed with passive radiation detectors mounted at 11 fixed locations within Columbus for the determination of the spatial distribution and long-term temporal evolution of the radiation field parameters. Due to their passive nature the detectors need to be returned to Earth for evaluation in the respective laboratories and also provide only integrated values of the dose received during their exposure. On the other hand, measurements are also carried out with two active radiation detectors mounted at a fixed position inside Columbus for the determination of the temporal variation of radiation field parameters. Due to their active nature they can provide near real-time information about the radiation field parameters. The long-term data gathered within the two experiments so far enables us to see variations of the radiation environment due to changes in solar activity, as well as due to altitude changes of the ISS.

2.1. DOSIS and DOSIS 3D experiments: hardware

The experiment hardware for DOSIS and DOSIS 3D experiments consists on the one hand of the so-called Passive Detector Packages (PDPs) consisting of thermoluminescence (TL), optically stimulated luminescence (OSL) detectors and nuclear track etch detectors (CR-39), which are put together in appropriate detector holders and sewed into Nomex Bags. These PDPs are mounted with adhesive Velcro strips at 11 locations within the Columbus Laboratory. Table 1 shows the PDPs location within Columbus, with the relevant related Research Racks and the coordinates, based on the Columbus coordinate system. The origin of the Columbus coordinate system is on the central axis of Columbus, where the module is connected to the ISS Node 2 (Axis orientations: $+X$ along the Columbus module axis toward the end cone (starboard side of the ISS), $+Y$ to Columbus forward side/ISS flight direction, $+Z$ to Columbus overhead/zenith) (EADS 2009).

Figure 2 provides a graphical illustration ("Fish Eye View") of the relevant detector locations, thereby showing that the locations are chosen in such a way as to enable a 3D dose distribution profile over the whole Columbus Laboratory. Figure 2 also provides the flight direction of the ISS and shows that five of the PDPs are located in the forward direction (see also PDP locations in italics in Table 1) while five of the PDPs are mounted in the backward direction of Columbus.

Table 1. Location of the PDPs within the Columbus Laboratory of the ISS.

PDP No.	Columbus location	Related rack	Position	Columbus coordinate system [mm]		
				X	*Y*	*Z*
1	Star Cone	–	Behind bend in right cone structure	681	−57	0
2	A4 UIP	HRF 2	Left side on UIP next to Vacuum connector	665	−123	−93
3	*F4 UIP*	*HRF 1*	*Left side on UIP next to Vacuum connector*	*570*	*123*	*−93*
4	*F4 HRF 1*	*HRF 1*	*B1 upper right panel*	*600*	*104*	*60*
5	A3 EPM	EPM	410 mm left from upper right edge	463	−104	93
6	A2 UIP	BLB	Left side on UIP next to Vacuum connector	436	−123	−93
7	O2 UIP	–	Left side on UIP next to Vacuum connector	436	−101	106
8	*F1 UIP*	*EDR*	*Left side on UIP next to Vacuum connector*	*243*	*123*	*−93*
9	*F1 EDR*	*EDR*	*77 mm left from upper right edge*	*333*	*104*	*93*
10	*End Cone*	–	*On PBA Cover*	*221*	*95*	*85*
X	DOSIS-MAIN-BOX	EPM	On the left side of the DOSIS-MAIN-BOX	516	−116	−60

Note. Positions given in italics (3 and 4 as well as 8–10) refer to the forward side of Columbus (see Fig. 2); HRF = Human Research Facility; EPM = European Physiology Module; EDR = European Drawer Rack; BLB = Biolab; PBA = Portable Breathing Apparatus; UIP = Utility Interface Panel.

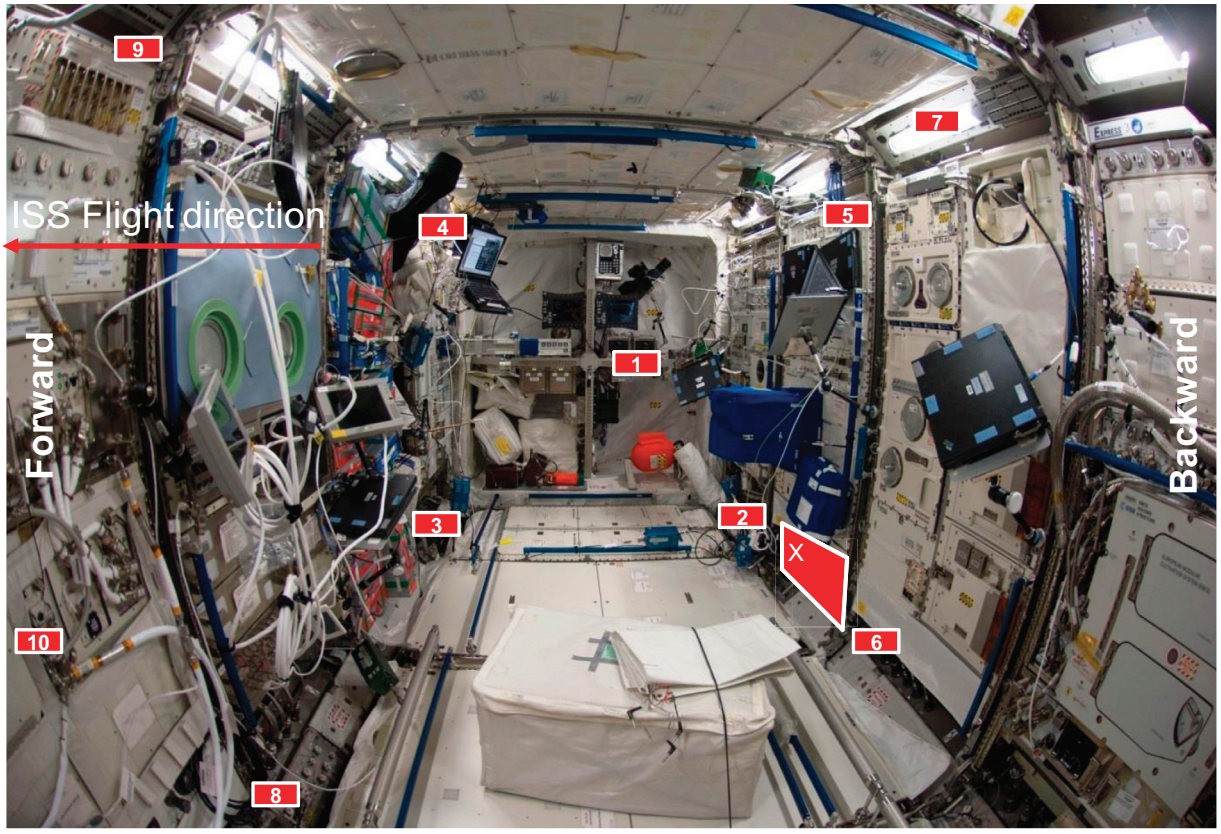

Fig. 2. The positions of the PDPs within the Columbus Laboratory of the ISS. PDP #3, 4, 8, 9, and 10 are positioned in forward and PDP # 1, 2, 5, 6, and 7 in backward Columbus position. The 11th PDP (X) is positioned at the large red rectangle beneath EPM attached to the DOSIS-MAIN-BOX (see also Fig. 3d). Source: NASA/ESA.

In addition, PDP #X (so-called Triple PDP) is mounted close to the active radiation detectors beneath the EPM, thereby also being positioned in the backward direction.

The active part of the DOSIS and DOSIS 3D hardware consists of two silicon detector telescopes (DOSTEL-1 and DOSTEL-2) looking in flight direction (DOSTEL-1) and perpendicular to the ISS flight direction (DOSTEL-2). The two instruments are connected over the so-called DOSTEL Data and Power Unit (DDPU) and mounted in a Nomex Box, called the DOSIS-MAIN-BOX, at a fixed position beneath the EPM rack. The DOSIS-MAIN-BOX is connected via a NASA 16 V Power Brick to an SUP outlet for the provision of power to the instruments. Data connection is done via the EPM LAN Interface at the upper right part of the EPM Facility. The scientific and housekeeping data are downloaded by the EPM rack via Ethernet connection with a nominal period of four weeks.

Figure 3 shows as example two PDPs mounted at location #1 (Star cone) (see Fig. 3a) and location #5 (EPM) (see Fig. 3b), the DOSIS-MAIN-BOX beneath EPM (Fig. 3c), and the Triple PDP mounted on the left side of the

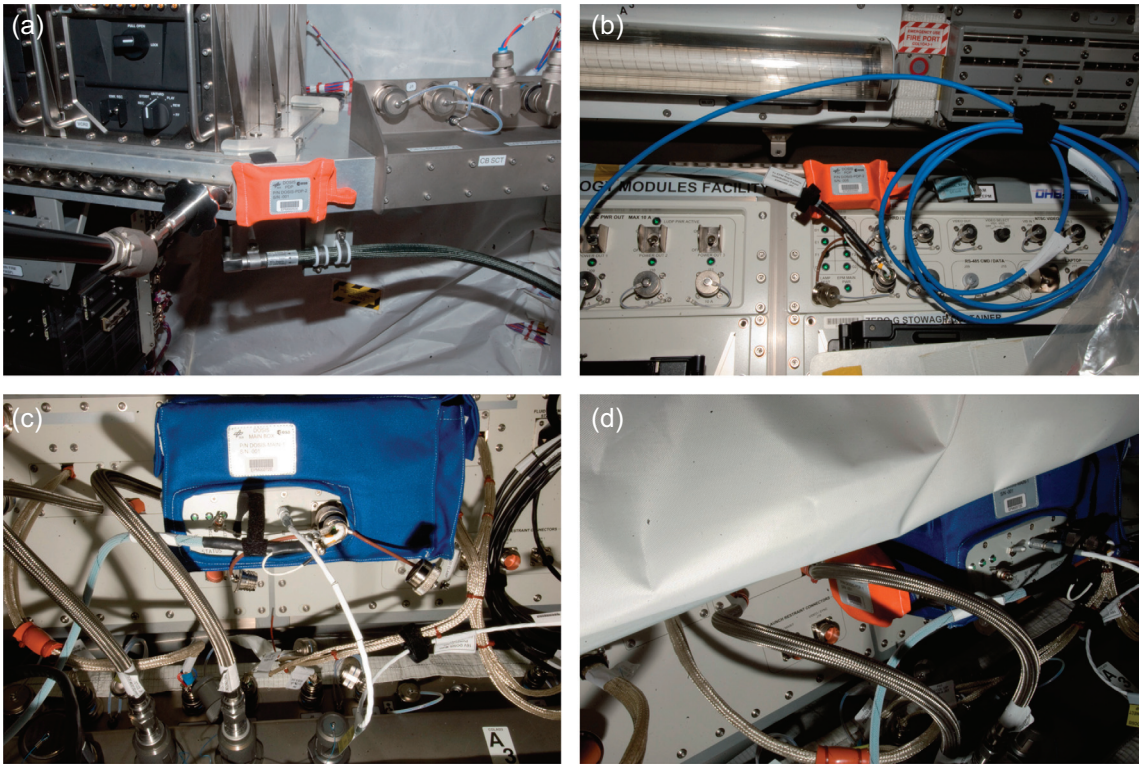

Fig. 3. DOSIS and DOSIS 3D hardware in the European Columbus Laboratory: (a) PDP #1 at star cone position; (b) PDP #5 at the upper part of the EPM facility; (c) DOSIS-MAIN-BOX with the two DOSTEL and the DDPU beneath the EPM Module; (d) Triple PDP mounted on the left side of the DOSIS-MAIN-BOX. Source: NASA/ESA.

Table 2. DOSIS and DOSIS 3D overall timeline.

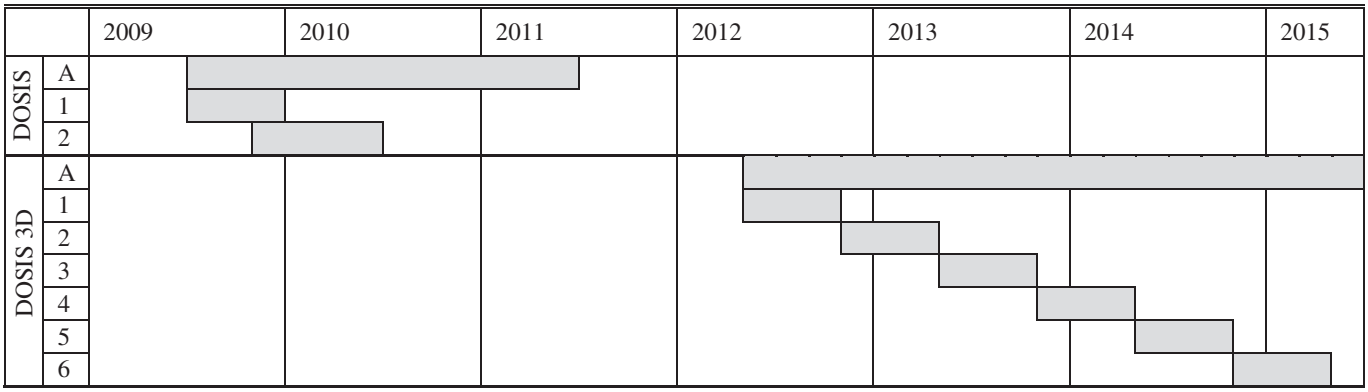

Note. A = active measurements; DOSIS 1 and 2 = passive measurement phases; DOSIS 3D 1–6 = passive measurement phases.

DOSIS-Main-Box (see Fig. 3d). Overall, with the active and passive detectors, the instrument suite provides a tremendous amount of data for the spatial and temporal variation of the radiation environment inside Columbus.

2.2. DOSIS and DOSIS 3D experiments: timeline

For the investigation of the spatial and temporal distribution of the radiation field inside the European Columbus module, the European Space Agency (ESA) experiments DOSIS (Dose Distribution Inside the ISS) (2009–2011) and DOSIS 3D (2012–onwards) were and are performed onboard the ISS. Within these two experiments eight sets of passive radiation detectors (DOSIS 1 and 2; DOSIS 3D 1–6) and two active radiation detectors (DOSTEL-1 and DOSTEL-2) measured the radiation environment over a wide timeframe. Table 2 gives a graphical overview of the relevant measurement periods for the active detectors (A) and the relevant passive detectors (DOSIS 1 and 2; DOSIS 3D 1–6).

A mission-related timeline for the passive radiation detectors is additionally shown in Table 3, while Table 4 provides the mission-related timeline for the active radiation detectors.

Table 3. Timeline for the passive detectors within the DOSIS and DOSIS 3D experiments.

Phase		Timeline		Duration [days]	Coverage [%]	ISS altitude [km]
DOSIS	1	Launch (STS-127)	July 15, 2009	136 (127)	93.3	339–348
		Installation	July 18, 2009			
		Retrieval	November 21, 2009			
		Return (STS-129)	November 27, 2009			
	2	Launch (STS-129)	November 16, 2009	191 (178)	93.2	337–349
		Installation	November 21, 2009			
		Retrieval	May 18, 2010			
		Return (STS-132)	May 26, 2010			
DOSIS 3D	1	Launch (Soyuz 30S)	May 15, 2012	125 (113)	90.4	397–417
		Installation	May 21, 2012			
		Retrieval	September 11, 2012			
		Return (Soyuz 30S)	September 17, 2012			
	2	Launch (Soyuz 32S)	October 23, 2012	144 (137)	95.1	407–416
		Installation	October 27, 2012			
		Retrieval	March 13, 2013			
		Return (Soyuz 32S)	March 16, 2013			
	3	Launch (Soyuz 34S)	March 28, 2013	167 (156)	93.4	407–416
		Installation	April 03, 2013			
		Retrieval	September 06, 2013			
		Return (Soyuz 34S)	September 11, 2013			
	4	Launch (Soyuz 36S)	September 25, 2013	167 (156)	93.4	413–418
		Installation	October 01, 2013			
		Retrieval	March 06, 2014			
		Return (Soyuz 36S)	March 11, 2014			
	5	Launch (Soyuz 38S)	March 25, 2014	170 (161)	94.7	407–416
		Installation	March 27, 2014			
		Retrieval	September 05, 2014			
		Return (Soyuz 38S)	September 11, 2014			
	6	Launch (Soyuz 40S)	September 26, 2014	167 (161)	96.4	413–418
		Installation	September 27, 2014			
		Retrieval	March 09, 2015			
		Return (Soyuz 40S)	March 12, 2015			

Table 4. Timeline for the active detectors within the DOSIS and DOSIS 3D experiments.

Detector		Timeline		Measurement period	Data [days]	ISS alt. [km]
DOSIS	DOSTEL-1 (1)	Launch (STS-127)	July 15, 2009	July 18, 2009–May 28, 2010	290	337–350
		Installation	July 18, 2009			
		Retrieval	April 21, 2011			
		Return (Soyuz 25S)	May 24, 2011			
	DOSTEL-2	Launch (STS-127)	July 15, 2009	July 18, 2009–June 16, 2011	645	337–375
		Installation	July 18, 2009			
		Retrieval	June 17, 2011			
		Return (STS-135)	July 21, 2011			
DOSIS 3D	DOSTEL-1/-2	Launch (Soyuz 30S)	May 15, 2012	May 21, 2012–March 15, 2015	969	398–418
		Installation	May 21, 2012		957	

(1) DOSTEL-1 stopped acquiring data after 290 measurement days in space on May 28, 2010.

DOSIS started with the launch of the first experiment suite (active and passive detectors) to the ISS on July 15, 2009 with the STS-127 Space Shuttle Endeavor. The passive radiation detectors were mounted within Columbus and were returned back to Earth with STS-129 Space Shuttle Atlantis at the end of November 2009. A second set of PDPs was launched with STS-129 and returned in May 2010 with STS-132 Space Shuttle Atlantis. This completed the first part of the DOSIS experiment with two long-term dose measurements with passive detectors within Columbus (see Table 3) from July 2009 to May 2010.

The second (active) part of the DOSIS experiment was mounted inside Columbus and activated on July 18, 2009. Consecutive measurements for the active part of the DOSIS project were performed up to May 28, 2010 for the DOSTEL-1 instrument (290 days) and up to June 16, 2011 with the DOSTEL-2 instrument (645 days) (see Table 4).

At the end of DOSIS, two passive detector exposure periods with 136 and 191 days were accomplished, as well as one long-term measurement period with the active DOSTEL-1 instrument of 290 days and one long-term measurement period with the active DOSTEL-2 instrument of 645 days. The active

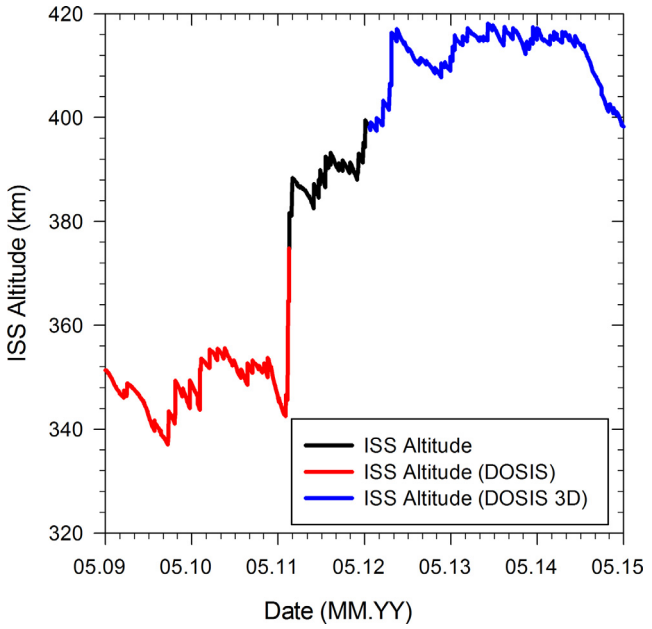

Fig. 4. The average ISS altitude over the time of the DOSIS (red) and DOSIS 3D (blue) experiments.

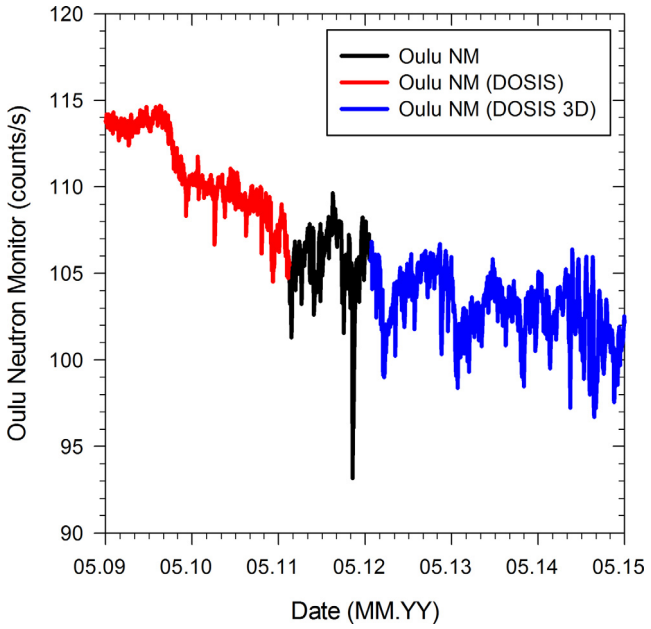

Fig. 5. The Oulu neutron monitor count rate over the time of the DOSIS (red) and DOSIS 3D (blue) experiments.

part of the hardware was returned to Earth with Soyuz 25S and STS-135 (Atlantis) for refurbishment for the upcoming DOSIS 3D experiment.

The DOSIS 3D experiment started on May 15, 2012 with the launch of the refurbished active radiation detectors (Table 4) and a new set of PDPs with the Soyuz 30S mission. In the framework of the DOSIS 3D project, the PDPs are up/down-loaded with each even number Soyuz flight, with an overall mission duration between 125 and 170 days (Table 3). Further on, Table 3 also gives the time the passive detectors were installed at relevant locations inside Columbus (see also Sect. 2.1). The overall percentage of time the detectors were installed at relevant positions accounts for between 93 and 96% of the overall mission duration.

Within the DOSIS 3D project, the active radiation detectors have been measuring for 969 (DOSTEL-1) and 957 (DOSTEL-2) days since the start of the experiment (Table 4).

2.3. DOSIS and DOSIS 3D solar cycle and space station altitude

Comparing the data from the DOSIS and DOSIS 3D experiments over a timespan of more than six years (2009–2015) requires the understanding of various parameters influencing the recorded doses as the ISS altitude and the solar cycle.

The temporal variation of the ISS altitude is given in Figure 4 for the DOSIS (in red) and the DOSIS 3D (in blue) experiment timeframes. The altitude ranged from 337 to 375 km for the DOSIS (see Fig. 4 in red) experiment up to the middle of June 2011. It is worthwhile to mention that during the last days of the active part of the DOSIS experiment in June 2011, the ISS started an altitude increase from ~340 km to over 375 km. For the DOSIS 3D (see Fig. 4 in blue) experiment starting in July 2012, the ISS altitude ranged from 398 to 417 km. Assuming similar shielding conditions, the contribution of Galactic Cosmic Ray particles is almost independent of the station altitude, whereas the fluence of trapped protons increases with altitude, also due to prolonged passages of the ISS through the South Atlantic Anomaly (SAA).

One other parameter influencing the radiation environment in LEO and the radiation load inside the ISS is the solar cycle. Due to enhanced deflection by the interplanetary magnetic field, increasing solar activity causes decreasing dose contribution from Galactic Cosmic Rays as well as for the protons in the South Atlantic Anomaly. To illustrate this, Figure 5 shows the Oulu neutron monitor count rate (http://cosmicrays.oulu.fi) for the DOSIS (in red) and DOSIS 3D (in blue) experiment timeframes. Whereas DOSIS (2009–2011) was performed in the deepest solar minimum conditions of the space age, especially in the year 2009, DOSIS 3D started in 2012 with already increasing solar activity and was running during solar maximum conditions in the years 2013 and 2014.

3. Detector systems

The detector systems used within DOSIS and DOSIS 3D are on the one hand passive integrating thermoluminescence (TL) (Sect. 3.1), optically stimulated luminescence (OSL) (Sect. 3.2), and nuclear track etch detectors (Sect. 3.3) and, on the other, active silicon detectors (Sect. 3.4). Passive detector systems have been used since the Mercury missions (Warren & Gill 1964) and especially the combination of luminescence detectors with nuclear track etch detectors is currently widely applied onboard the ISS because it allows not only the determination of the absorbed dose, but also the dose equivalent in combining these two detector systems (see for example: Vanhavere et al. 2008). Active silicon detector systems are commonly used onboard the ISS (see also Narici et al. 2015), and therefore offer good baseline data for intercomparison purposes.

3.1. Passive detectors: thermoluminescence detectors (TLDs)

Within the DOSIS and DOSIS 3D experiments, the following thermoluminescence detectors (TLDs) were applied by the relevant groups.

DLR, Cologne, Germany, and ATI, Vienna, Austria, used extruded ribbons of ^{6}LiF:Mg,Ti (TLD-600) and ^{7}LiF:Mg,Ti

(TLD-700) and single crystals of CaF_2:Tm (TLD-300) detectors available from Thermo Fisher Scientific Inc., Waltham, MA, USA (former Harshaw Chemical Co., Solon, OH, USA), with the dimensions $3.2 \times 3.2 \times 0.9$ mm^3.

National Institute of Radiological Sciences (NIRS), Chiba, Japan, used TLD-100 (^{Nat}LiF:Mg,Ti), provided by Nagase Landauer Ltd., Japan. The size is $3 \times 3 \times 0.9$ mm^3. NASA/SRAG, Houston, USA, used single crystal chips of ^{Nat}LiF:Mg,Ti (TLD-100) and CaF_2:Tm (TLD-300) detectors available from Thermo Scientific Inc., Waltham, MA, USA, with the dimensions $3.2 \times 3.2 \times 0.9$ mm^3.

IFJ, Krakow, Poland, applied self-produced pellets of ^{6}LiF:Mg,Ti (MTS-6), ^{7}LiF:Mg,Ti (MTS-7), and ^{7}LiF:Mg,Cu,P (MCP-7) with 4.5 mm diameter and 0.6 mm thickness. MTA EK used pellets of ^{6}LiF:Mg,Ti (MTS-6) and ^{7}LiF:Mg,Ti (MTS-7) with 4.5 mm diameter and 0.9 mm thickness, produced by the Institute of Nuclear Physics (IFJ), Krakow, Poland.

SCK·CEN, Mol, Belgium used thin square pellets of ^{6}LiF:Mg,Ti (MTS-6) and ^{7}LiF:Mg,Ti (MTS-7) with dimensions $3.2 \times 3.2 \times 0.9$ mm^3 and thin disk-shaped pellets of ^{6}LiF:Mg,Cu,P (MCP-6) and ^{7}LiF:Mg,Cu,P (MCP-7) with 4.5 mm diameter and 0.9 mm thickness, all produced by IFJ, Krakow, Poland. NPI, Prague, Czech Republic, used $CaSO_4$:Dy detectors ($CaSO_4$:Dy powder fixed by thermostable silicon binder in aluminum dishes) (Guelev et al. 1994) of the type Protecta MMS, manufactured by Laboratories Protecta Ltd., and single crystals of Al_2O_3:C (TLD-500 K) from Ural State University (Akselrod et al. 1990); both types of TLDs with 5 mm diameter and 1 mm thickness.

The relevant readout procedures and protocols for the applied detectors are given in Table 5. As can be seen, there are some differences in experimental details, as each laboratory used its own procedure, based on its experience and practice. It has previously been demonstrated that, in spite of such differences, the obtained results are consistent and agree well within measurement uncertainties (Berger et al. 2013; Bilski et al. 2013). The measured thermoluminescent signals were converted to units of absorbed dose in water through calibrations performed with secondary-standard gamma-ray radiation sources (^{60}Co for ATI, SCK·CEN and ^{137}Cs for DLR, IFJ, NIRS, MTA EK, NPI, NASA/SRAG).

3.2. Passive detectors: optically stimulated luminescence detectors (OSLDs)

All OSLDs used in this experiment were prepared from the same Al_2O_3:C material used in the Luxel^{TM} and InLight^{TM} dosimetry systems and provided by Landauer Inc.

Nevertheless, each laboratory used its own preparation (bleaching) and readout procedure and equipment. It has been shown that the experimental readout parameters (e.g., choice of signal, optical filters used, etc.) influence the relative response of the OSLDs as a function of the linear energy transfer (LET) and, therefore, may result in slightly different doses in mixed heavy charged particle (HCP) fields (Sawakuchi et al. 2008). To assist in the comparison of the results, Table 6 summarizes the detector preparation, readout, and analysis protocols used by the individual laboratories.

The OSLDs from OSU are $4 \times 4 \times 0.3$ mm^3 detectors, bleached overnight under a yellow light (fluorescent lamp filtered by Schott GG-495) to erase any signal accumulated during storage. The detectors were read out for 600 s to record the OSL signal S during space exposure. They were then individually irradiated with a reference dose D_R from at ^{90}Sr/^{90}Y that is part of the Risø reader and again read to obtain the reference signal S_R. The ^{90}Sr/^{90}Y source was calibrated using the same type of detector and experimental condition against a ^{60}Co source at the National Institute of Standards and Technology (NIST) in gamma dose to water. The dose was then calculated (see Eq. (1)).

$$M(\mathrm{Gy}) = \frac{S}{S_R} D_R. \quad (1)$$

The reference dose D_R must be larger than the doses to which the detectors were exposed, to avoid the influence of sensitivity changes in the detector (Yukihara et al. 2006). Another option is to obtain the full S/S_R versus dose calibration curve, which takes into account sensitivity changes in the detector. For the dose levels reported here, we found that the results using these different methodologies differ by less than 1%. The Belgian Nuclear Research Center (SCK·CEN) used disk-shaped Al_2O_3:C (Luxel^{TM}) OSLDs with 4.8 mm diameter and 0.2 mm thickness. For bleaching, the OSLDs are exposed to daylight for one day. The readout is done with green light from an argon ion laser. The OSL signal is calculated either as the maximum of or the area under the decay curve. The optically stimulated luminescence material (i.e., Luxel^{TM}) used by NASA/SRAG for the DOSIS project is identical to that used by the previous groups. The OSL measurements were performed using a Risø TL/OSL-DA-15C/D reader that uses, as light stimulation source, a 525 nm green diode module with a total power at the dosimeter of ~40 mW/cm^2. The OSL signal was measured using 7.5 mm Hoya-U340 filters to allow for proper discrimination between the stimulation and emission light (Gaza et al. 2006). The NIRS used an OSLD (Al_2O_3:C) provided by Nagase Landauer Ltd., Japan. The size of this OSLD is 7.2 mm in diameter with 0.5 mm in thickness.

3.3. Passive detectors: nuclear track etch detectors

Nuclear Track Etch Detectors were used by DLR, MTA EK, NPI, IFJ, NIRS, and NASA/SRAG during all of the DOSIS and DOSIS 3D missions. The relevant detector materials and experimental protocols used by the individual laboratories for detector preparation and readouts are summarized in Table 7.

The CR-39 track etch detectors used at DLR are made of polyallyl-diglycol-carbonate ($C_{12}H_{18}O_7$) and manufactured by American Technical Plastics Inc. (ATP), USA. The detectors were chemically etched in a NaOH solution (6.25 N, 50 °C) for 36 and 168 h in a two-step etching process. The resulting tracks are analyzed manually using a Leitz Metalloplan microscope with a PixeLINK digital camera using DLR developed software (Straube et al. 2010).

The used track etch detectors from MTA EK were produced by Track Analysis Systems Ltd. (TASL). Bristol, UK. A two-step etching process is applied: after the short etching (6 h), high LET particle tracks become visible, while the longer etching (15 h) reveals the lower LET particles as well. The different geometric parameters of the particle tracks are examined, using a Polyvar microscope (Reichert-Jung AG, Austria) equipped with a digital complementary metal-oxide semiconductor (CMOS) camera, in semi-automatic measurement mode, except the high-energy and high-charge (HZE) particles, which are measured manually. The image analysis

Table 5. TLD readout, annealing, and calibration procedures applied by the DOSIS/DOSIS 3D participants.

Institute	TLD name	Readout system	Heating Rate [°C/s]	Material	Preheat	Annealing cycle	Cooling rate	Calibration method	Calibration source	Glow curve evaluation
DLR	TLD-600/-700 TLD-300	Harshaw 5500 (Hamamatsu RC095 HA)	5	LiF:Mg,Ti	No preheat	400 °C (1 h), 100 °C (2 h)	Slow	The same single-chip	^{137}Cs	Peak 5 height
				CaF_2:Tm	No preheat	400 °C (1 h), 100 °C (2 h)	Slow			Peak 5 height
ATI	TLD-600/-700 TLD-300	TL-DAT.II (THORN EMI 9635 QB)	5	LiF:Mg,Ti	120 °C (30 min)	400 °C (1 h)	Slow	The same single-chip	^{60}Co	Peak 5 height
				CaF_2:Tm	No preheat	400 °C (1.5 h)	Slow			Peak 5 height
IFJ (1)	MTS-6 MTS-7 MCP-7	RA'94 (THORN EMI 9789 QB) + Harshaw 3500 (ET 9125B)	10	LiF:Mg,Ti	120 °C (30 min)	400 °C (1 h), 100 °C (2 h)	Fast	Seperate group of TLDs	^{137}Cs	Peak integral
				LiF:Mg,Cu,P	120 °C (30 min)	240 °C (10 min)	Fast			Peak integral
SCK·CEN (2)	MTS-6 MTS-7 MCP-6 MCP-7	Harshaw 5500 (Hamamatsu RC095 HA)	1	LiF:Mg,Ti	No preheat	400 °C (1 h), 100 °C (2 h)	Slow	Separate group of TLDs from the same batch	^{60}Co	Peak integral
				LiF:Mg,Cu,P	No preheat	240 °C (10 min)	Fast			Peak integral
MTA EK (3)	MTS-6 MTS-7	Harshaw 2000 A-B, PC (Thorn EMI 9235QA)	10	LiF:Mg,Ti	No preheat	400 °C (1 h), 100 °C (2 h)	Fast	The same single-chip	^{137}Cs	Peak 5 height
NIRS	TLD-100	Harshaw 5500 (Hamamatsu RC095 HA)	25	LiF:Mg,Ti	No preheat	400 °C (1 h), 100 °C (2 h)	Slow	The same batch	^{137}Cs	Peak 5 Integral
NASA/ SRAG	TLD-100 TLD-300	Harshaw 5500 (Hamamatsu RC095 HA)	6	LiF:Mg,Ti	100 °C (30 min)	400 °C (1 h)	Slow	The same batch	^{137}Cs	Peak 5 height
				CaF_2:Tm		400 °C (1 h), 100 °C (2 h)	Fast			Peak 5 integral
NPI	Al_2O_3:C $CaSO_4$:Dy	RA'94 (THORN EMI 9789 QB) + TOLEDO 654 TLD Reader	10	Al_2O_3:C	No preheat	700 °C (20 min)	Fast	The same single-chip	^{137}Cs	Glow curve integral
				$CaSO_4$:Dy	150 °C (22 s)	380 °C (10 min)	Fast			

(1) IFJ used RA'94 reader for the DOSIS and Harshaw 3500 reader for the DOSIS 3D experiments.
(2) SCK·CEN TLD Glow curve evaluation for peak integral: 100 °C–260 °C (MTS) and 170 °C–230 °C (MCP).
(3) MTA EK started providing TLDs with the start of the DOSIS 3D experiment.

Table 6. OSLD preparation: all groups applied Al_2O_3:C (Luxel) detectors.

Institute	Readout system	Power [mW/cm^2]	Filter	Stimulation Time [s]	Bleaching	Calibration Method	Source	OSL curve evaluation
OSU	Risø TL/OSL-DA-15C/D (Green diodes: 525 nm)	13.3	7.5 mm Hoya-U340	600	Yellow light over night	Single "chip"	^{90}Sr/^{90}Y (calib. against ^{60}Co)	(2)
SCK·CEN	Homemade (Ar+ laser: 488 nm)	120	Melles Griot 01MCG019	100	No (daylight)	Separate group from the same batch	^{60}Co	
NASA/SRAG	Risø TL/OSL-DA-15C/D (Green diodes: 525 nm)	40	7.5 mm Hoya-U340	300	Bleached with 525 nm for 120 s	Same batch	^{137}Cs	(3)
NIRS	MicroStar InLight (Landauer Inc.) (Green diodes: 525 nm)	173 (1)	7.5 mm Hoya-B390	1	Fluorescent light without UV	Same batch	^{137}Cs	

(1) Calculated value from nominal specification of employed LEDs.
(2) Total OSL area (300 s or 600 s stimulation at 10 mW/cm^2).
(3) OSL initial intensity (3 s) or total OSL area (300 s) at 40 mW/cm^2.

Table 7. Overview of the CR-39 evaluation, etching, and analyzing procedure.

Institute	Manufacturer/trade name	Etching time [hours]	Etching temperature [°C]	NaOH conc. [N]	Bulk layer [μm]	Analyzed area [cm^2]
DLR	ATP	36/168	50	6.25	8.83/50	0.14/0.1
MTA EK	TASTRAK	6/15	70	6	8.04/20.1	0.5/0.5
NPI	HARZLAS TD-1	18	70	5	15.3	0.09
IFJ	TASTRAK	12	70	7	20.89	0.12
NIRS	HARZLAS TD-1 TechnoTrak	8	70	7	14.7	0.0404
NASA/SRAG	ATP	38	60	6.25	24.29	0.03

and data processing are performed by MTA EK developed software, which determines the LET spectrum for each etching step, using the method described in Pálfalvi (2009). To obtain the final LET spectra, the results from the measurements of the short and long etched detectors are combined. Absorbed dose rates (D) in water, dose equivalent rates (H), and averaged quality factors (Q) are calculated following the recommendations given in NCRP Report No. 137 (2001) and Pálfalvi (2009).

The Nuclear Physics Institute (NPI), Prague, Czech Republic, used HARZLAS TD-1 (Nagase Landauer Ltd.) detectors with a thickness of 0.9 mm. After etching in 5 N NaOH at 70 °C for 18 h, the tracks are imaged and analyzed using the system HSP-1000 and software HspFit (Pachnerová Brabcová et al. 2013).

The Institute of Nuclear Physics (IFJ), Krakow, Poland, used 0.7 mm thick TASTRAK detectors (Track Analysis Systems Ltd. (TASL), Bristol, UK). After etching in 7 N water solution of NaOH at 70 °C for 12 h, the tracks are imaged using a Leitz Metalloplan microscope with a PixeLINK digital camera and analyzed using ImageTool software.

The NIRS used CR-39 (HARZLAS/TD-1) provided by Nagase Landauer Ltd., Japan and CR-39 (TechnoTrak) provided by Chiyoda Technol Corp., Japan. Their detector size is typically 18 × 16 × 0.9 mm^3. After chemical etching with 7N NaOH at 70 °C for 8 h, the nuclear tracks are imaged and analyzed using the system HSP-1000 and software HspFit (Yasuda et al. 2005).

The CR-39 track etch detectors used at NASA/SRAG are manufactured by American Technical Plastics Inc. (ATP), USA. The CR-39 track etch detectors are chemically etched in a NaOH solution (6.25N, 60 °C ± 5 °C) for 38 h. The resulting tracks are analyzed manually using a Zeiss Axioskop 40 optical microscope. The bulk etch is calculated using the mass difference before and after etching (Zhou et al. 2007a, 2007b).

3.4. Active detectors DOSTEL

The Dosimetry Telescope (DOSTEL) instrument applied within DOSIS and the DOSIS 3D project has its heritage from numerous space missions (Reitz et al. 1998; Beaujean et al. 1999a, 1999b; Reitz et al. 1999; Beaujean et al. 2002; Reitz et al. 2005; Labrenz et al. 2015). The DOSTEL instrument is based on two passivated implanted planar silicon (PIPS) detectors each with a thickness of 315 μm and an area of 6.93 cm^2 arranged in a telescope geometry. The detectors are mounted at a distance of 15 mm, yielding a telescope with a

geometric factor of 824 mm^2 sr for particles in coincidence mode. With this detector configuration, the DOSTEL measures count rates and dose rates of radiation hitting a detector ("dose measurement") and coincidental hits in the two detectors to limit the pathlength in the detectors to derive information about the LET ("telescope" or "LET" measurement). Based on the measured data, DOSTEL provides absorbed dose and dose equivalent values. Due to the fact that two DOSTEL instruments are mounted in perpendicular positions, information about the directionality of the radiation field inside Columbus can also be determined.

4. Results and discussion

Within the eight experiment phases of the DOSIS (Phase 1 and 2) and DOSIS 3D (Phase 1–Phase 6) experiments over the years 2009–2015, a tremendous amount of data has been gathered. The current evaluation and discussion of the results gathered within these eight experiment phases will be divided into four steps and will only focus on the passive TL/OSL detectors with a short comparison of results gathered with the active radiation detector system. The first step is the detailed comparison of data produced by all TL/OSL detectors for one experiment phase of the DOSIS 3D experiment (Phase 2). All the relevant conclusions drawn for the TL/OSL comparison for this phase are of course also valid for the other experiment phases. The second step will show the full dataset for the eight experiment phases using exemplarily data from ^{6}LiF:Mg,Ti and ^{7}LiF:Mg,Ti detectors provided by ATI, DLR, IFJ, SCK·CEN, and MTA EK. The third step will compare ^{7}LiF:Mg,Ti data gathered within two DOSIS 3D phases in Columbus with data from NASA/SRAG taken at other locations inside the ISS. The fourth step will compare data measured with passive TLDs with data provided by one of the active DOSTEL instruments (DOSTEL-1) for the whole duration of the relevant exposure phases in the years 2009–2015.

4.1. DOSIS 3D 2: TLD/OSL data for one experiment phase – in-depth comparison

For the comparison of the different TL/OSL materials one full dataset of results from the DOSIS 3D Phase 2 (October 2012–March 2013) (see Table 3) experiment was taken as an example. Figure 6 and Tables 8 and 9 provide an overview of the relevant absorbed dose rate values measured by ATI, IFJ, SCK·CEN, DLR, MTA EK, NPI, NASA/SRAG, and OSU for all applied TL/OSL materials.

Figure 6 combines the datasets for ^{6}LiF:Mg,Ti; ^{7}LiF:Mg,Ti; CaF_2:Tm; ^{Nat}LiF:Mg,Ti; ^{6}LiF:Mg,Cu,P; ^{7}LiF:Mg,Cu,P; Al_2O_3:C (OSL); Al_2O_3:C (TLD), and $CaSO_4$:Dy in several subplots, providing at the same time the comparison of the relevant data for each research group working with the relevant detector material.

It is clear that the data obtained by different groups with the same detector type agree quite well: in almost all cases, the measured absorbed dose rates agree within the statistical uncertainties. At the same time, there are substantial differences between absorbed doses measured with various detector materials. One reason for this difference lies in the distinct relative OSL/TL-efficiency to heavy charged particles (protons, helium up to iron), which constitute a large portion of the radiation environment onboard the ISS.

Studies relating to this have been carried out at various accelerator facilities around the world mimicking as close as possible the radiation field and its constituents in space. Especially during the ICCHIBAN experiments a tremendous amount of comparison data has been gathered providing a better way of interpreting the results (Uchihori & Benton 2004). Based on the knowledge of the differences in OSL/TL-efficiency, all the relevant results and their differences can be explained.

For example, it was found that $CaSO_4$:Dy applied by the NPI has a much higher efficiency to heavy ions than the applied Al_2O_3:C material from the NPI (Spurny & Jadrnickova 2008). With this knowledge, the differences in the TL readings (on average, around 9% higher for $CaSO_4$:Dy) can be explained. The same applies to the difference in LiF:Mg,Ti and LiF:Mg,Cu,P detectors used by the IFJ and SCK·CEN. On average, the values for ^{7}LiF:Mg,Ti are 15% (IFJ) and 18% (SCK·CEN), higher than those for the applied ^{7}LiF:Mg,Cu,P detectors (Bilski 2006; Berger & Hajek 2008; Bilski & Puchalska 2010; Bilski et al. 2011; Bilski et al. 2016). The LiF:Mg,Ti and LiF:Mg,Cu,P response ratio is also discussed further in Section 4.2. The TL-efficiency for CaF_2:Tm is slightly higher than that for the nominally applied ^{7}LiF:Mg,Ti (Hajek et al. 2008; Berger & Hajek 2008), which gives comparable results for the ATI and DLR applied CaF_2:Tm detectors and the ^{7}LiF:Mg,Ti ones.

The comparison of ^{7}LiF and ^{6}LiF data reveals that the latter are systematically higher. This indicates the presence of the neutron-induced signal, due to the ^{6}Li isotope, which possesses a very high cross-section for (n, α) reactions with thermal and epithermal neutrons. The observed difference between ^{7}LiF:Mg,Ti and ^{6}LiF:Mg,Ti data is on average below 20 μGy/day, which amounts to about 5% of the total ^{6}LiF signal. The same comment applies to the difference in ^{6}LiF:Mg,Cu,P and ^{7}LiF:Mg,Cu,P material with an average of 13 μGy/day. It should be emphasized that this value is not the real neutron-absorbed dose, but rather a gamma-ray dose that would be needed to produce a thermoluminescent signal of equal intensity (sometimes called "gamma-equivalent neutron dose") (see also Berger et al. 2013). ^{Nat}LiF:Mg,Ti containing 7.5% of ^{6}Li produced typical dose values in between those of highly enriched ^{7}LiF/^{6}LiF detectors. No significant differences of the neutron signal between PDP locations were observed.

The OSL data from OSU and SCK·CEN agree reasonably well, considering the differences attributed to the experimental readout conditions. SCK·CEN uses blue-light stimulation and a filter that detects only (or mostly) F-center luminescence in Al_2O_3:C, whereas OSU uses green-light stimulation and the Hoya U-340 filter that transmits signals from both the F and F+-centers in Al_2O_3:C. As shown earlier, the relative luminescence efficiency will depend on the experimental readout conditions, including the choice of filters (that allows or not the detection of Al_2O_3:C UV emission band) and the choice of signal (initial part of the OSL curve or the entire OSL curve) (Sawakuchi et al. 2008). Comparing OSU results, which are based on the total OSL area, with SCK·CEN results for the total OSL area, OSU results are typically higher by 8–27% (average of 15%). Based on the data from Sawakuchi et al. (2008), relative luminescence efficiencies when the UV center emission is detected are 2.9–39.3% higher than when the UV center emission is not detected, with an average of 19.2% between the different experiments (of course, this simple average does not take into account the actual composition of the space radiation

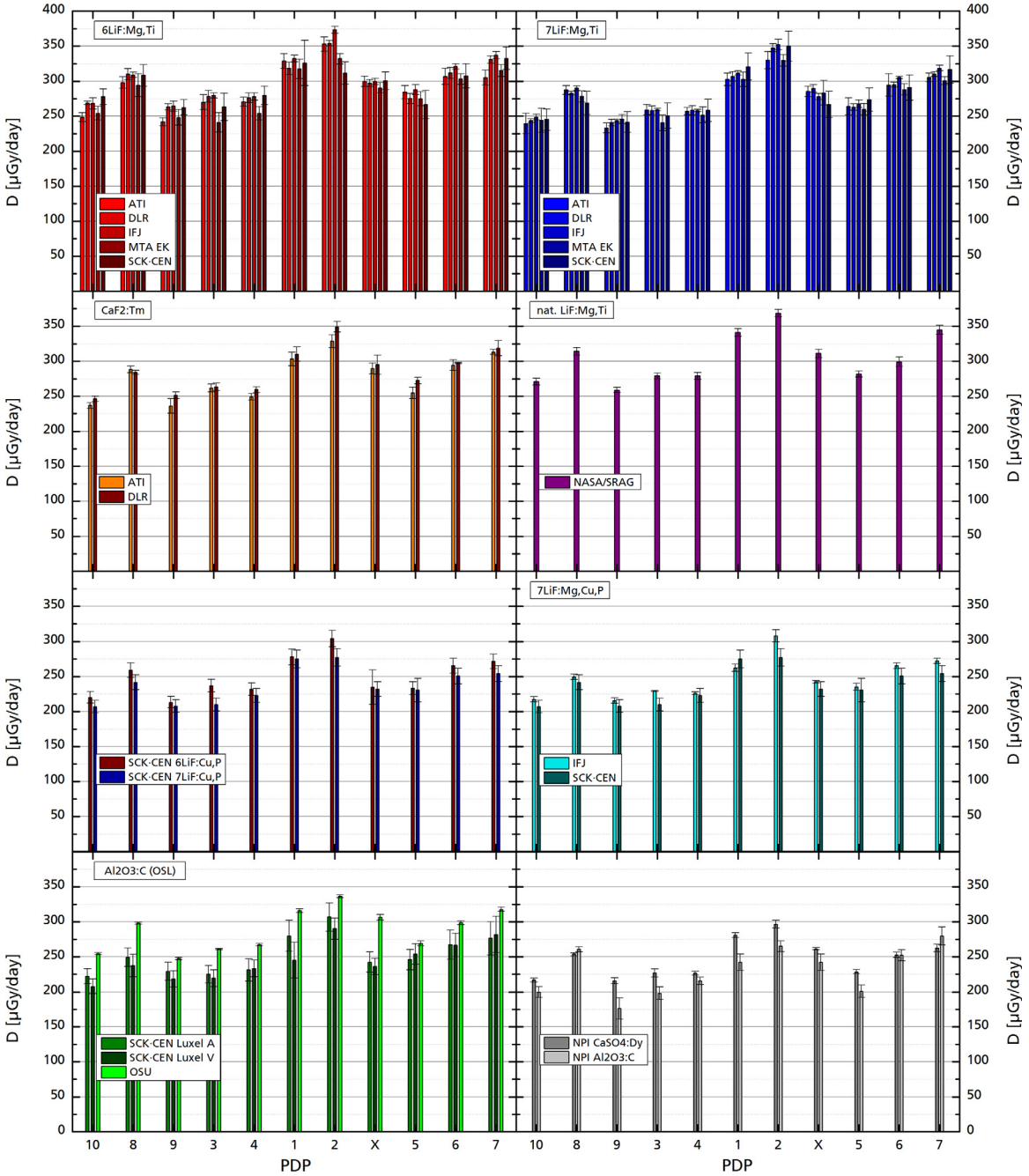

Fig. 6. Summary of the results for all TLD/OSL detector materials for DOSIS 3D Phase 2 (October 2012–March 2013). The PDP numbering for the horizontal axes is based on the locations of the PDPs in the Columbus Laboratory, starting with location #10 at the left entry of Columbus following the locations on the Columbus forward side up to PDP #1 and coming back to the Columbus backward side, ending at PDP position #7.

environment). The important finding, however, is that both OSU and SCK·CEN data follow the same pattern, as can be observed in Figure 6.

The use of Hoya U-340 filters by OSU has been based on better agreement with ^{6}LiF:Mg,Ti results. Comparing OSU results with ^{6}LiF:Mg,Ti results in Figure 6, this assumption seems to be confirmed.

In summary, all these investigations concerning the relevant changes in OSL/TL-efficiency as well as the contribution of thermal and epithermal neutrons to the readings of ^{6}Li detectors explain in detail the behavior of the absorbed dose rates for the relevant detector materials, especially if one looks at the data from the "working horse" of TLDs, namely the ^{7}LiF:Mg,Ti detector values. For the relevant mission phase, the absorbed dose rates measured with ^{7}LiF:Mg,Ti range from around 250 µGy/day for at the lowest dose rate positions (PDP positions #10, #9, #3, and #4) up to around 350 µGy/day at the highest dose rate position (PDP position #2). In comparison, the values measured with Al_2O_3:C (TL) are around 200 µGy/day for the lowest dose values and around 260 µGy/day for the highest, and the respective positions inside Columbus, which account for a decrease of around 20% in measured dose. Table 10 and Figure 7 further illustrate this statement by presenting the ratios of the absorbed dose measured with a given material to that of ^{7}LiF:Mg,Ti, clearly

Table 8. LiF:Mg,Ti results for the DOSIS 3D Phase 2 experiment.

	Absorbed dose rate [μGy/d]										
PDP	^{6}LiF:Mg,Ti					^{7}LiF:Mg,Ti					^{Nat}LiF:Mg,Ti
	DLR	ATI	IFJ	SCK·CEN	MTA EK	DLR	ATI	IFJ	SCK·CEN	MTA EK	NASA/SRAG
1	318 ± 9	329 ± 10	332 ± 5	326 ± 32	317 ± 14	307 ± 7	298 ± 16	312 ± 3	321 ± 19	303 ± 10	331 ± 3
2	354 ± 4	353 ± 10	373 ± 5	312 ± 16	332 ± 8	348 ± 6	321 ± 13	352 ± 7	350 ± 22	330 ± 8	358 ± 3
3	279 ± 8	270 ± 11	280 ± 4	263 ± 19	241 ± 14	258 ± 6	259 ± 8	259 ± 2	251 ± 18	240 ± 11	271 ± 2
4	276 ± 7	271 ± 6	278 ± 5	280 ± 13	254 ± 10	258 ± 7	254 ± 9	258 ± 2	258 ± 16	252 ± 12	271 ± 3
5	275 ± 7	284 ± 9	288 ± 7	267 ± 20	275 ± 10	263 ± 5	255 ± 15	268 ± 5	274 ± 17	260 ± 8	274 ± 2
6	312 ± 8	307 ± 11	321 ± 4	308 ± 17	303 ± 8	295 ± 4	290 ± 16	305 ± 2	291 ± 18	288 ± 8	314 ± 4
7	331 ± 5	305 ± 11	337 ± 5	333 ± 16	315 ± 8	310 ± 4	303 ± 9	319 ± 4	317 ± 19	301 ± 6	335 ± 5
8	310 ± 8	298 ± 8	309 ± 4	308 ± 15	294 ± 16	283 ± 3	288 ± 14	290 ± 3	269 ± 17	278 ± 8	299 ± 6
9	263 ± 5	242 ± 5	264 ± 7	263 ± 11	248 ± 11	241 ± 4	227 ± 14	244 ± 2	242 ± 15	246 ± 6	251 ± 2
10	269 ± 2	249 ± 6	268 ± 8	278 ± 11	254 ± 10	244 ± 3	233 ± 15	249 ± 4	245 ± 15	244 ± 17	263 ± 3
X	297 ± 5	300 ± 7	299 ± 5	301 ± 13	291 ± 7	290 ± 5	285 ± 8	278 ± 4	267 ± 19	283 ± 18	302 ± 4

Table 9. CaF_2:Tm; LiF:Mg,Cu,P; Luxel and $CaSO_4$:Dy and Al_2O_3:C results for the DOSIS 3D Phase 2 experiment.

	Absorbed dose rate [μGy/d]									
PDP	CaF_2:Tm		^{6}LiF:Mg, Cu,P	^{7}LiF:Mg, Cu,P	^{7}LiF:Mg, Cu,P	Luxel	Luxel$^{(Area)}$	Luxel$^{(Vmax)}$	$CaSO_4$:Dy	Al_2O_3:C
	DLR	ATI	SCK·CEN		IFJ	OSU	SCK·CEN		NPI	
1	304 ± 9	310 ± 10	278 ± 11	275 ± 13	262 ± 5	316 ± 3	280 ± 22	245 ± 26	281 ± 4	242 ± 11
2	339 ± 22	349 ± 8	304 ± 12	277 ± 13	308 ± 9	337 ± 2	307 ± 20	290 ± 15	297 ± 5	265 ± 8
3	259 ± 10	264 ± 5	237 ± 9	210 ± 9	229 ± 1	261 ± 1	225 ± 13	219 ± 12	227 ± 6	198 ± 9
4	245 ± 7	260 ± 4	232 ± 9	223 ± 10	226 ± 2	267 ± 2	231 ± 16	233 ± 12	227 ± 3	215 ± 5
5	248 ± 9	272 ± 5	233 ± 9	231 ± 17	235 ± 5	269 ± 4	246 ± 15	254 ± 15	229 ± 3	201 ± 9
6	292 ± 10	298 ± 1	265 ± 10	251 ± 11	265 ± 4	299 ± 3	267 ± 21	267 ± 17	253 ± 4	252 ± 8
7	316 ± 5	319 ± 11	272 ± 10	254 ± 11	272 ± 4	318 ± 3	276 ± 24	282 ± 26	263 ± 5	280 ± 13
8	285 ± 8	284 ± 3	259 ± 10	242 ± 10	249 ± 4	298 ± 1	249 ± 13	238 ± 16	254 ± 2	261 ± 4
9	231 ± 10	251 ± 5	213 ± 8	208 ± 9	216 ± 4	248 ± 2	229 ± 13	218 ± 12	216 ± 4	176 ± 15
10	235 ± 5	246 ± 4	220 ± 8	207 ± 9	217 ± 4	255 ± 2	222 ± 11	208 ± 10	217 ± 3	200 ± 8
X	293 ± 11	295 ± 14	235 ± 25	232 ± 10	242 ± 2	307 ± 4	242 ± 15	236 ± 12	262 ± 2	242 ± 11

Table 10. Ratio of various TL/OSL data to ^{7}LiF:Mg,Ti data.

Material	Ratio
^{6}LiF:Mg,Ti	1.06
^{Nat}LiF:Mg,Ti	1.06
^{6}LiF:Mg,Cu,P	0.90
^{7}LiF:Mg,Cu,P	0.87
Al_2O_3:C (OSL)	1.04
CaF_2:Tm	1.01
$CaSO_4$:Dy	0.88
Al_2O_3:C (TL)	0.82

demonstrating that for the interpretation of dosimetric values gained with passive luminescence detectors in Low Earth Orbit (LEO), one has to clearly understand the detector material.

4.2. DOSIS and DOSIS 3D: TLD data for eight experiment phases

The second part aims at the comparison of data gathered during the two DOSIS and the six DOSIS 3D experiment phases. For the absorbed dose, values shown in the following Figures 8–11 are taken from ATI, IFJ, SCK·CEN, and DLR for DOSIS and from ATI, IFJ, SCK·CEN, MTA EK, and DLR for the DOSIS 3D experiment phases.

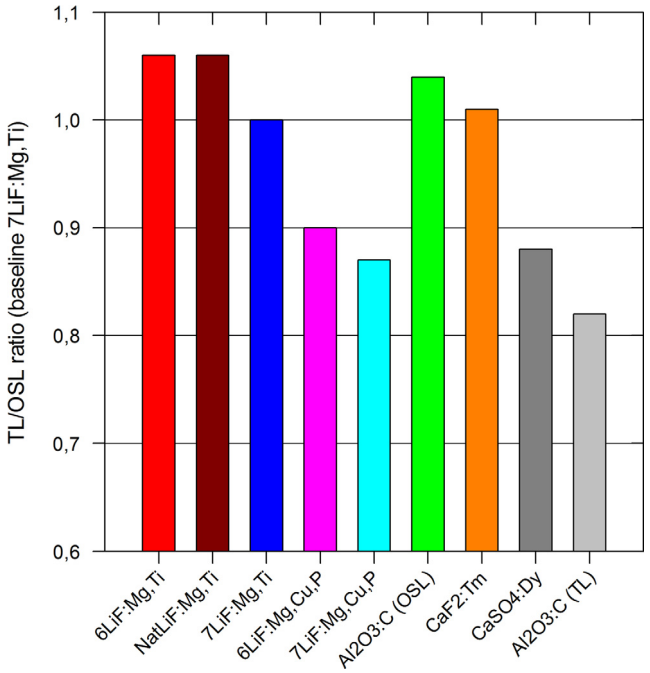

Fig. 7. TL/OSL ratio for the relevant applied detector materials normalized to ^{7}LiF:Mg,Ti detector data.

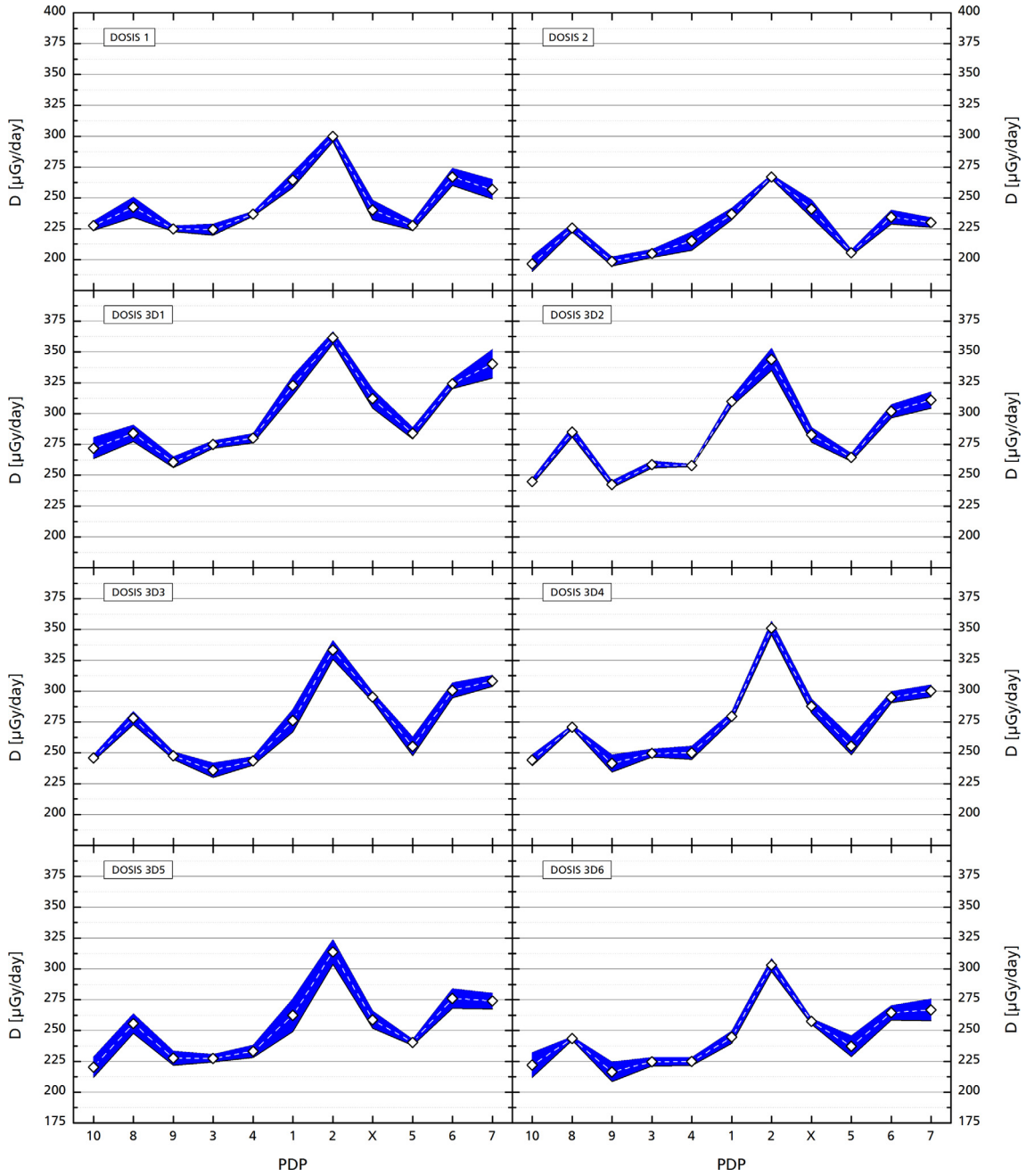

Fig. 8. ^{7}LiF:Mg,Ti data for the two DOSIS (DOSIS 1 and DOSIS 2) and the six DOSIS 3D (DOSIS 3D1 to DOSIS 3D6) experiment phases. The blue band represents the weighted standard error of the mean.

Figure 8 provides the mean values with the respective uncertainties for the ^{7}LiF:Mg,Ti detector material, while Figure 9 provides the same data for ^{6}LiF:Mg,Ti for all eight exposure phases. As can be seen, the mean value of ^{6}LiF:Mg,Ti is always, as expected and further explained in Section 4.1, higher than the respective ^{7}LiF:Mg,Ti data. The higher spread in ^{6}LiF:Mg,Ti detector data compared to the ^{7}LiF:Mg,Ti data is based on various reasons. One is the fact that the groups used ^{6}LiF:Mg,Ti detectors of different thicknesses. The detectors were also stacked (up to six detectors in one stack). Different thicknesses of ^{6}LiF:Mg,Ti, especially in a stacked configuration, can lead to different absorption and self-absorption of the thermal and epithermal neutrons (Burgkhardt et al. 2006), thereby decreasing the neutron signal to detectors below or in between. This was observed not only in various space missions (Berger et al. 2013), but also during aircraft measurements (Berger et al. 2008).

For all eight exposure missions (Fig. 8), we see a similar pattern of absorbed dose rate over the 11 positions in Columbus. The reason for this pattern lies in the different local shielding thicknesses for the 11 PDP positions inside the Columbus Laboratory. Changes in the local shielding configuration mostly influence the contributions to the absorbed dose values due to the low-energy protons of the South Atlantic Anomaly crossings.

For DOSIS 1 and DOSIS 2, the absorbed dose values are in the range between 200 and 300 µGy/day, with a reduction in dose from DOSIS 1 to DOSIS 2 due to a slow increase in solar activity. From DOSIS 2 to DOSIS 3D 1, we observe a sharp increase in dose rates (with minima at around 260 µGy/day

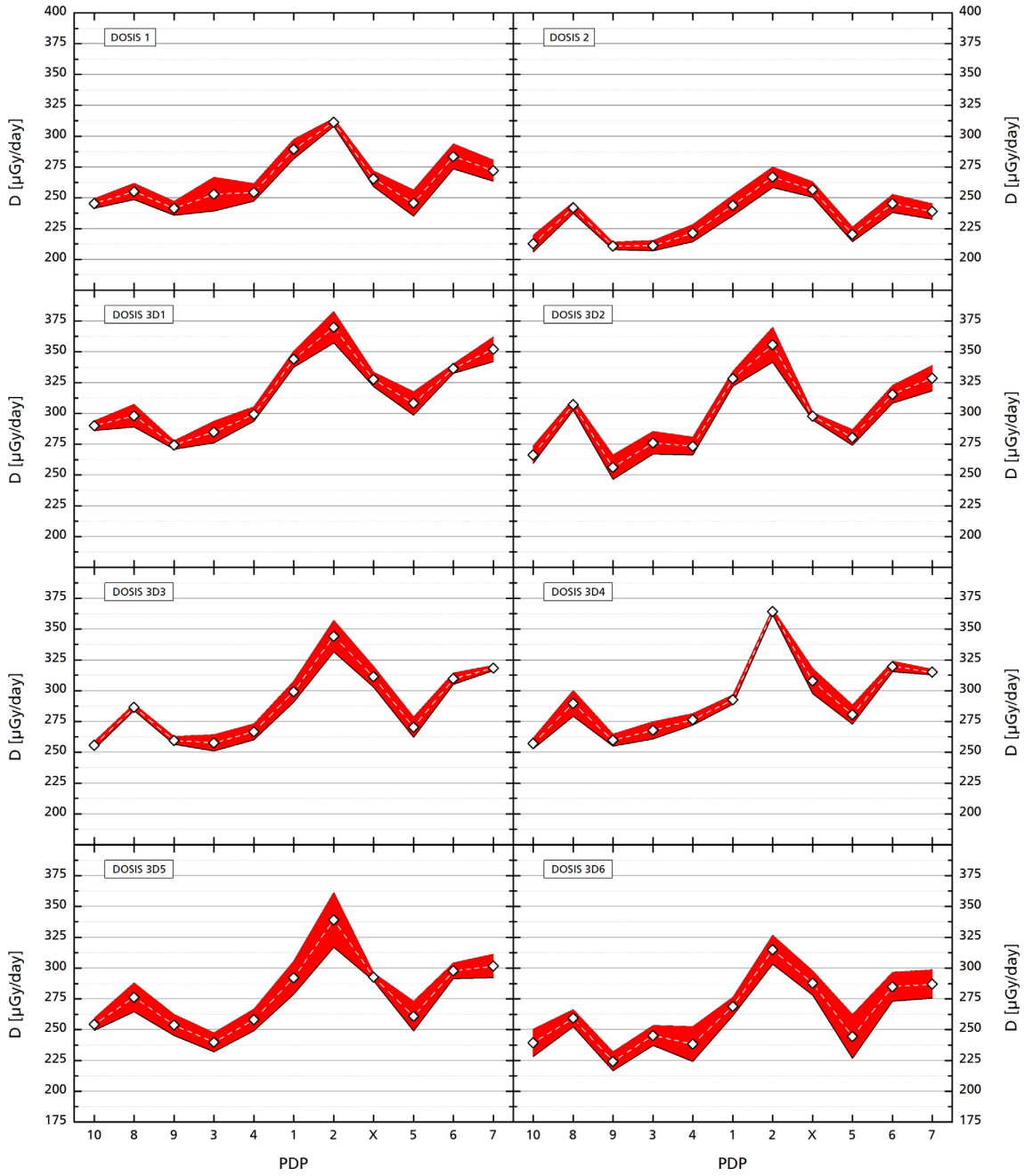

Fig. 9. ^{6}LiF:Mg,Ti data for the two DOSIS (DOSIS 1 and DOSIS 2) and the six DOSIS 3D (DOSIS 3D1 to DOSIS 3D6) experiment phases. The red band represents the weighted standard error of the mean.

and maxima up to 360 µGy/day), which can be attributed to the increase in ISS altitude by more than 70 km in the year 2011, resulting in higher contributions of protons from the South Atlantic Anomaly Crossings. From DOSIS 3D 1 onwards, the ISS altitude remained high, but solar activity increased further up to solar maximum in the years 2013–2014, leading to a reduction in trapped and galactic cosmic ray contributions. For DOSIS 3D 6, in the beginning of 2015, we arrive at similar dose values as for DOSIS 1 in 2009. This illustrates again the need for long-term dose monitoring and the influence of solar activity and ISS altitude on the doses onboard the ISS.

The variation discussed before is further illustrated in Figure 10. It gives the mean as well as the range of dose values measured with ^{7}LiF:Mg,Ti detectors for all relevant mission phases in relation to the changes in the space radiation environment (from solar minimum to solar maximum) as well as to the changes in the altitude of the ISS.

As can be seen over the time of the DOSIS 3D missions, the dose rate gradually decreased due to increases in solar activity, and at the end of DOSIS 3D Phase 6, it almost reached the same levels as for the DOSIS 1 Phase.

Figure 11 shows the variation of ^{7}LiF:Mg,Ti data separated in the forward and backward PDP positions in Columbus. Figure 11a gives the data for the forward PDPs, while Figure 11b shows the data for the backward positioned PDPs. It is clearly seen that the absorbed dose rate in the forward direction is lower for all DOSIS and DOSIS 3D experiment phases than the dose for the backward direction.

Recently, the dependence of the response ratio LiF:Mg,Ti to LiF:Mg,Cu,P on the cosmic radiation spectrum was studied

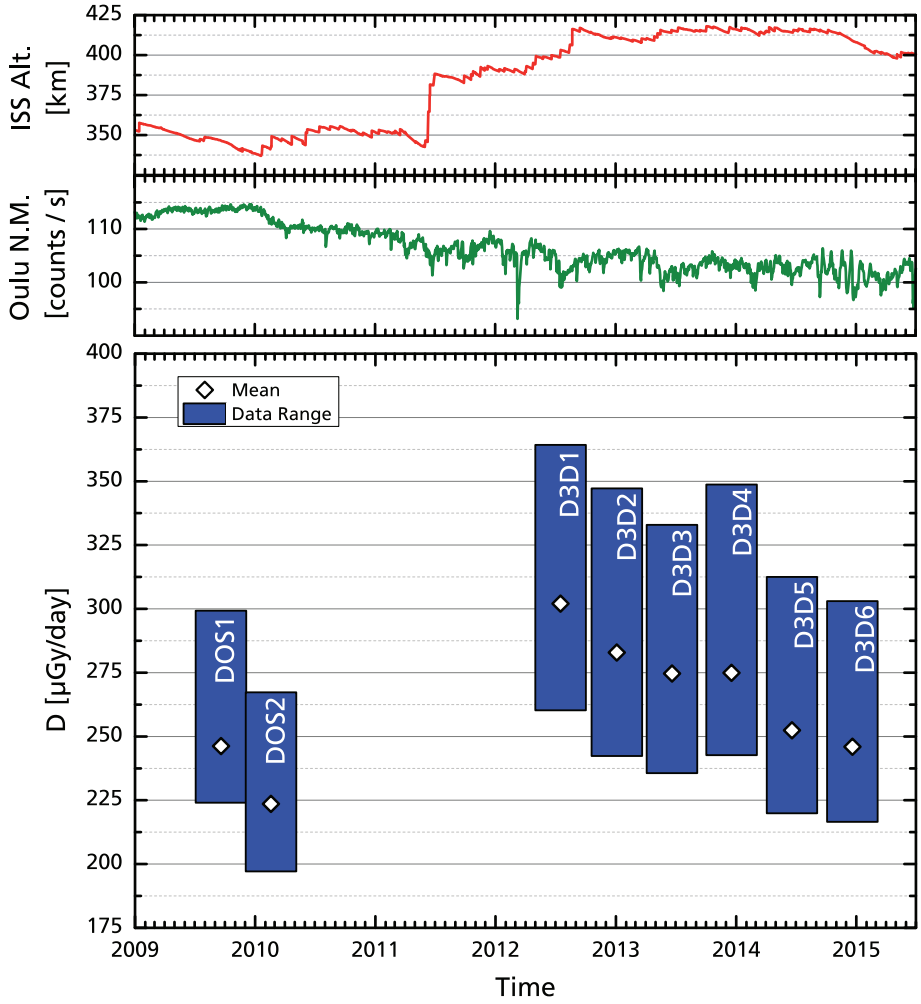

Fig. 10. ^{7}LiF:Mg,Ti data (mean, minimum and maximum) for two DOSIS (DOS1 and DOS2) and the six DOSIS 3D (D3D1 to D3D6) experiment phases. In addition, the plot gives the changes in ISS altitude and the relevant Oulu NM count rates.

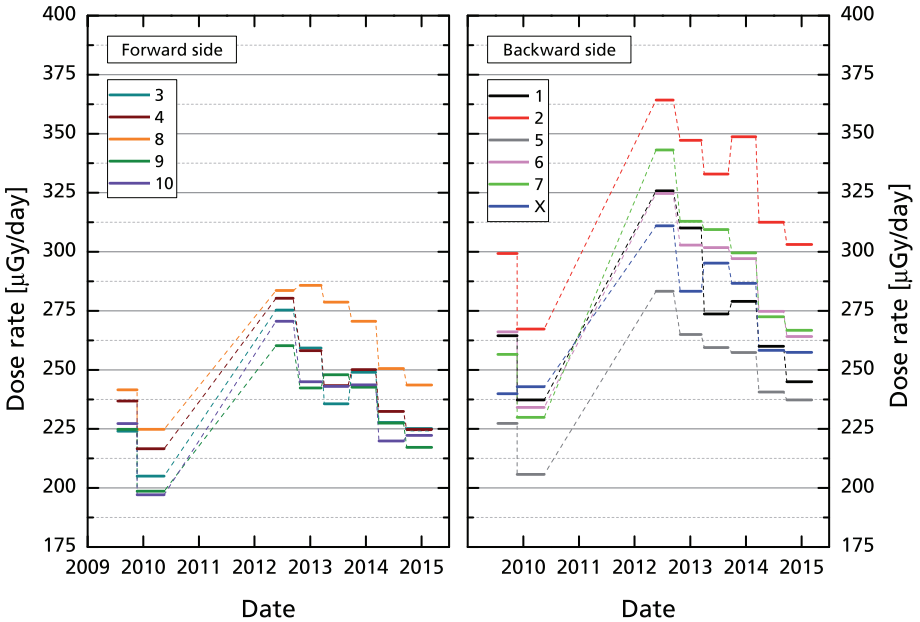

Fig. 11. ^{7}LiF:Mg,Ti data (mean) for the two DOSIS (DOSIS 1 and DOSIS 2) and the six DOSIS 3D (DOSIS 3D1 to DOSIS 3D6) experiment phases for the forward side (a) and the backward side (b) of Columbus.

Table 11. Timeline for one NASA/SRAG ISS RAM exposure phase.

	Timeline		Duration [days]	Coverage [%]	ISS altitude [km]
NASA/SRAG ISS RAM	Launch (Soyuz 38S)	March 25, 2014	229 (218)	95.1	On average ~415.3
	Installation	April 02, 2014			
	Retrieval	November 06, 2014			
	Return (Soyuz 39S)	November 10, 2014			

Table 12. NASA/SRAG ISS RAM Locations and respective dose values.

	NASA/SRAG ISS RAM location		Total mission dose [mGy]	Absorbed dose rate [μGy/d]
1	LAB1_D3	Inside of WORF rack, in the vicinity of the Lab D3 window	96.44 ± 2.75	421 ± 12
2	LAB1_OS0	Closeout panel on the starboard side of forward hatch, upper edge of panel	55.27 ± 1.42	241 ± 6
3	LAB1_D4	CheCS RSR centered on the inner side of D2 locker door.	46.23 ± 1.20	201 ± 5
4	A/L1 AD3	Aft wall, low outboard in large section	87.04 ± 2.60	380 ± 11

Note. LAB = US Laboratory (Destiny); WORF = Window Observational Research Facility; CheCS = Crew Health Care System; A/L = Airlock.

(Bilski et al. 2016). It was found that this ratio is especially influenced by the shielding thickness, decreasing with increasing thickness. The values measured within the DOSIS missions fluctuate around 1.15, which is fairly consistent with the predictions for the Columbus module (Bilski et al. 2016) and corresponds to the effective shielding of about 50 g/cm^2. The differences between various positions of PDPs are rather small, suggesting that the effective shielding is probably mainly dominated by the mass of the Columbus module and the whole station, and less influenced by local shielding. Nevertheless, some PDP locations seem to show systematically somewhat higher or lower values, suggesting effects of local shielding. For example, the lowest value of this ratio was nearly always found for PDP #3, while the highest for PDP #7 and these locations correspond to the lowest and to the highest measured dose rates.

4.3. DOSIS 3D: TLD data from other parts of the ISS

This third chapter provides additional ^{7}LiF:Mg,Ti (TLD-700) data from NASA/SRAG for their nominal applied Radiation Area Monitoring (RAM) devices used by NASA/SRAG throughout the Station. For the comparison with DOSIS 3D data, an overlapping time period was used as given in Table 11.

The ISS RAM detectors were launched with Soyuz 38S and remained installed for a total mission time of 229 days for returning back with Soyuz 39S. This time period would cover the DOSIS 3D Phase 5 (March–September 2014) as well as the first part of DOSIS 3D Phase 6 (September 2014–March 2015). Within these two time periods, the ^{7}LiF:Mg,Ti data for Columbus ranged from 216 ± 8 to 313 ± 9 μGy/day. Data from NASA/SRAG is provided for four positions outside of Columbus (see Table 12). While Positions 1–3 were inside the US LAB (Destiny), Position 4 was in the Airlock.

Table 12 provides the total absorbed mission dose as well as the absorbed dose rates in μGy/day for these four respective positions. In comparison to the dose values in Columbus, we see similar minima of the absorbed dose rate 201 ± 5 μGy/day, but also an increased maximum of 421 ± 12 μGy/day at the location close to the LAB D3 window, which can be attributed to lower shielding close to the window. Overall, the additional data confirms that within the relevant modules, the dose values can vary up to a factor of 2, depending on the local shielding environment.

4.4. DOSIS and DOSIS 3D: TLD/DOSTEL comparison

This section shows a comparison between the measurements of the active DOSTEL-1 instrument and the passive ^{7}LiF:Mg,Ti detectors mounted close to it for the DOSIS and DOSIS 3D experiments. Figure 12 provides, as an example, the count rate (counts/sec) measured with one of the DOSTEL instruments for a time period of 12 h. It shows the nominal and expected behavior for a silicon detector onboard the ISS, with the variations in counts related to the Galactic Cosmic Rays over the nominal orbits of the ISS and the additional spikes (on average up to six per day) for the crossings of the South Atlantic Anomaly (SAA) (see for example: Reitz et al. 2005; Labrenz et al. 2015). Figure 13 provides in addition the corresponding absorbed dose rate in silicon for this 12-h time period, with the minima at the equator of between 1 and 2 μGy/h followed by the respective maxima at high northern and southern geomagnetic latitudes of up to 20 μGy/h and the highest dose rates due to the SAA crossings with up to 300 μGy/h.

With the DOSTEL instrument, due to its active dosimetry data, one is able to distinguish between contributions from GCR and SAA to the total absorbed dose. For example, during Phase 2 of the DOSIS experiment, the average DOSTEL-1 absorbed dose rate accounted for 234 ± 18 μGy/day (see Table 13), with contributions from GCR of 150 μGy/day and a contribution from the on average 4–6 daily SAA crossings of 84 μGy/day. For DOSIS 3D Phase 1 with the increase in ISS altitude (see also Fig. 4), the daily absorbed dose values account for 286 ± 25 μGy/day with contributions from GCR of 145 μGy/day, and a contribution from the SAA crossings of 141 μGy/day. With this, the SAA contribution increased by around 75% due to the changes in ISS altitude. In terms of comparison with other active radiation detectors onboard the ISS, one can state that the absorbed dose rates measured with the DOSTEL-1 instruments are in line with data provided by the Russian DB-8 instrument located in the Russian Zvezda Module of the ISS (Lishnevskii et al. 2012), taking into

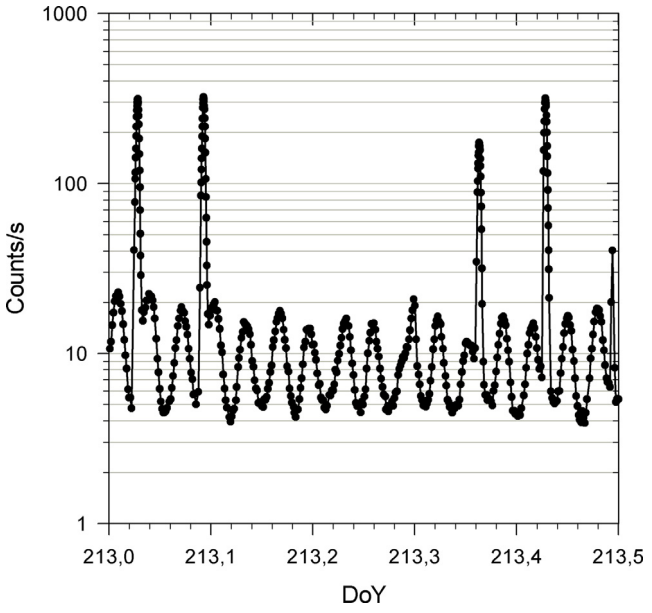

Fig. 12. Count rate profile of the DOSTEL-1 instrument for 12 h.

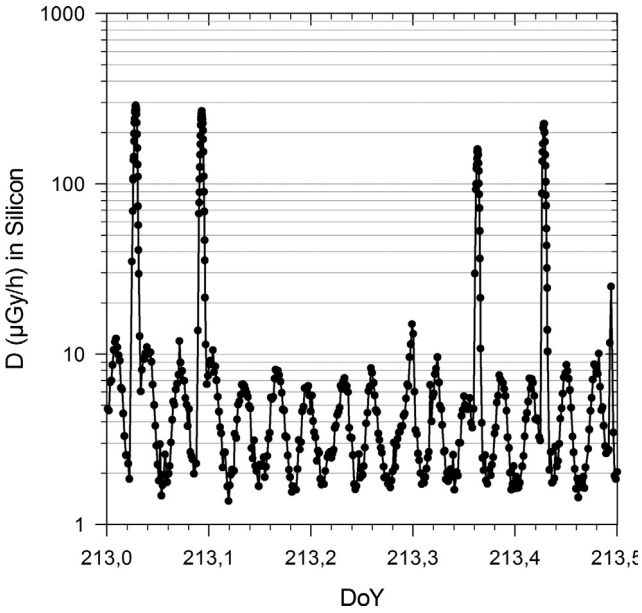

Fig. 13. Absorbed dose rate (µGy/h) in Silicon profile of the DOSTEL-1 instrument for 12 h.

Table 13. Comparison of the daily dose rate measured with the DOSTEL-1 instrument with data from ^{7}LiF:Mg,Ti detectors for DOSIS Phase 1 and 2 and the DOSIS 3D Phase 1–6.

Experiment	Phase	Duration	ISS altitude [km]	Absorbed dose rate [µGy/d]	
				DOSTEL-1	^{7}LiF:Mg,Ti
DOSIS	1	July 15, 2009–November 27, 2009	339–348	248 ± 20	261 ± 21
	2	November 16, 2009–May 26, 2010	337–349	234 ± 18	238 ± 10
DOSIS 3D	1	May 15, 2012–September 17, 2012	397–417	286 ± 25	311 ± 9
	2	October 23, 2012–March 16, 2013	407–416	288 ± 20	281 ± 9
	3	March 28, 2013–September 11, 2013	407–416	297 ± 23	294 ± 7
	4	September 25, 2013–March 11, 2014	413–418	294 ± 23	294 ± 12
	5	March 25, 2014–September 09, 2014	413–417	279 ± 22	262 ± 7
	6	September 26, 2014–March 12, 2015	401–416	256 ± 20	256 ± 7

account the different shielding thicknesses the four DB-8 units have inside the Russian part of the ISS.

For the entire DOSIS and DOSIS 3D missions, one PDP (Triple PDP) was always attached at the left side of the DOSIS-MAIN BOX (see Fig. 3d). Table 13 provides a comparison of the absorbed dose data (converted to absorbed dose in water) measured with the DOSTEL-1 instrument with the ^{7}LiF:Mg,Ti data provided by the Triple PDP located around 15 cm from the DOSTEL-1 instrument. DOSTEL-1 data was therefore averaged over the relevant mission duration as given in Table 3. As can be seen, the data agrees very well within the respective error bars. In addition, it should be noted that (a) the PDP was located directly at the DOSIS-MAIN BOX only between 93 and 96% of the mission time (see Table 3), with the rest of the mission time either flying to the ISS or already stowed for return from the ISS, and (b) the DOSTEL instruments measure with almost 100% efficiency in a wider LET range than the TLDs, while the TL-efficiency starts dropping above around 10 keV/µm. However, the newest calculations by Bilski et al. (2016) show that ^{7}LiF:Mg,Ti would still measure, in terms of absorbed dose in water, about 95% of the relevant dose inside the ISS.

5. Summary and conclusion

In the framework of the DOSIS (2009–2011) and the DOSIS 3D (2012-ongoing) experiments, the spatial and temporal variation of the radiation environment in the European Columbus Laboratory onboard the ISS has been and is still being mapped with a variety of active and passive radiation detectors. The passive radiation detectors (TLD and OSLD) enabled determination of the variation of the absorbed dose rates at 11 positions inside Columbus, with data from eight research groups providing in total a number of 10 different TLD/OSLD materials. This provided a direct comparison of the absorbed dose rate gathered with these different materials and, due to extensive ground-based calibration efforts, enabled the explanation of differences in the relevant absorbed dose readings. Data measured with passive radiation detectors showed that the absorbed dose values inside the Columbus Laboratory follow a pattern, based on the local shielding configuration of the radiation detectors, with minimum dose values observed in the year 2010 of 195–270 µGy/day and maximum values observed in the year 2012 with values ranging from 260 to 360 µGy/day. The absorbed dose is modulated by (a) the variation in solar activity and (b) the changes in ISS altitude.

In summary, the data inside Columbus shows variations of up to 50%. A comparison with data gathered by the active DOSTEL-1 instrument over the mission phases showed close agreement of the absorbed dose values measured by the active systems and data from the passive ^{7}LiF:Mg,Ti detectors. The database generated up to now will be further expanded to include data from the combination of the passive TLD/OSLD systems with the Nuclear Track Etch Detectors and further comparison with the active systems.

Acknowledgements. The participation of the Technische Universität Wien, Atominstitut (ATI), Vienna, Austria in the DOSIS-1 and -2 experiments was supported by the Austrian Space Applications Programme (ASAP) under Contract No. 819643. The Polish contribution for the Institute of Nuclear Physics (IFJ), Krakow, Poland was supported by the National Science Center (Project No DEC-2012/06/M/ST9/00423). MTA EK greatly acknowledges the possibility of participating in the project to the DLR and to the ESA PECS for the Financial Grant No. PECS4000108464. The participation of the Nuclear Physics Institute of the Czech Academy of Sciences was supported by the grant of Czech Science Foundation (GACR) No. 15-16622Y. The CAU, University of Kiel was supported by DLR under Grants 50WB0826, 50WB1026, 50WB1232, and 50WB1533.

The authors would like to thank the Sodankyla Geophysical Observatory and the website teams (http://cosmicrays.oulu.fi) for providing the Oulu neutron monitor data.

The authors gratefully acknowledge the support of the European Space Agency (ESA) especially Jason Hatton, Rene Demets, Chiara Lombardi, and Liesbeth De Smet, as well as colleagues from CADMOS, Toulouse, France and DLR-MUSC, Cologne, Germany. All of these experiments would not have been possible without the help of all the astronauts working on the DOSIS and s: Frank de Winne, Tracy Caldwell-Dyson, Shannon Walker, Ron Garan, Mike Fossum, Andre Kuipers, Joe Acaba, Sunita Williams, Chris Hadfield, Chris Cassidy, Luca Parmitano, Michael Hopkins, Rick Mastracchio, Koichi Wakata, Alexander Gerst, Samantha Cristoforetti, and Scott Kelly.

The editor thanks Karel Kudela and an anonymous referee for their assistance in evaluating this paper.

References

Akselrod, M.S., V.S. Kortov, D.J. Kravetsky, and V.I. Gotlib. Highly sensitive thermoluminescent anion-defective α-Al2O3:C single crystal detectors. *Radiat. Prot. Dosim.*, **32 (1)**, 15–20, 1990.

Beaujean, R., J. Kopp, and G. Reitz. Active dosimetry on recent space flights. *Radiat. Prot. Dosim.*, **85 (1–4)**, 223–226, 1999a.

Beaujean, R., G. Reitz, and J. Kopp. Recent European measurements inside Biorack. *Mutat. Res.*, **430 (2)**, 183–189, 1999b, DOI: 10.1016/S0027-5107(99)00129-3.

Beaujean, R., J. Kopp, S. Burmeister, F. Petersen, and G. Reitz. Dosimetry inside MIR station using a silicon detector telescope (DOSTEL). *Radiat. Meas.*, **35 (5)**, 433–438, 2002, DOI: 10.1016/S1350-4487(02)00074-4.

Berger, T. Radiation dosimetry onboard the International Space Station ISS. *Z. Med. Phys.*, **18 (4)**, 265–275, 2008, DOI: 10.1016/j.zemedi.2008.06.014.

Berger, T., and M. Hajek. TL-efficiency – overview and experimental results over the years. *Radiat. Meas.*, **43 (2–6)**, 146–156, 2008, DOI: 10.1016/j.radmeas.2007.10.029.

Berger, T., M. Meier, G. Reitz, and M. Schridde. Long term dose measurements applying a human anthropomorphic phantom onboard an aircraft. *Radiat. Meas.*, **43 (2–6)**, 580–584, 2008, DOI: 10.1016/j.radmeas.2007.12.004.

Berger, T., P. Bilski, M. Hajek, M. Puchalska, and G. Reitz. The MATROSHKA experiment: results and comparison from EVA (MTR-1) and IVA (MTR-2A/2B) exposure. *Radiat. Res.*, **180 (6)**, 622–637, 2013, DOI: 10.1667/RR13148.1.

Berger, T., M. Hajek, P. Bilski, and G. Reitz. Cosmic radiation exposure of biological test systems during the EXPOSE-R mission. *Int. J. Astrobiol.*, **14 (1)**, 27–32, 2015, DOI: 10.1017/S1473550414000548.

Bilski, P. Response of various LiF thermoluminescent detectors to high energy ions: results of the ICCHIBAN experiment. *Nucl. Instrum. Methods B*, **251 (1)**, 121–126, 2006, DOI: 10.1016/j.nimb.2006.05.012.

Bilski, P., and M. Puchalska. Relative efficiency of TL detectors to energetic ion beams. *Radiat. Meas.*, **45 (10)**, 1495–1498, 2010, DOI: 10.1016/j.radmeas.2010.05.013.

Bilski, P., T. Berger, M. Hajek, and G. Reitz. Comparison of the response of various TLDs to cosmic radiation and ion beams: current results of the HAMLET project. *Radiat. Meas.*, **46 (12)**, 1680–1685, 2011, DOI: 10.1016/j.radmeas.2011.03.023.

Bilski, P., T. Berger, M. Hajek, A. Twardak, C. Koerner, and G. Reitz. Thermoluminescence fading studies: implications for long-duration space measurements in Low Earth Orbit. *Radiat. Meas.*, **56**, 303–306, 2013, DOI: 10.1016/j.radmeas.2013.01.045.

Bilski, P., T. Berger, and D. Matthiä. Influence of cosmic radiation spectrum and its variation on the relative efficiency of LiF thermoluminescent detectors – calculations and measurements. *Radiat. Meas.*, **88**, 33–40, 2016, DOI: 10.1016/j.radmeas.2016.02.029.

Burgkhardt, B., P. Bilski, M. Budzanowski, R. Bottger, K. Eberhardt, G. Hampel, P. Olko, and A. Straubing. Application of different TL detectors for the photon dosimetry in mixed radiation fields used for BNCT. *Radiat. Prot. Dosim.*, **120 (1–4)**, 83–86, 2006, DOI: 10.1093/rpd/nci597.

Caffrey, J.A., and D.M. Hamby. A review of instruments and methods for dosimetry in space. *Adv. Space Res.*, **47 (4)**, 563–574, 2011, DOI: 10.1016/j.asr.2010.10.005.

Durante, M., and F.A. Cucinotta. Physical basis of radiation protection in space travel. *Rev. Mod. Phys.*, **83**, 1245–1281, 2011, DOI: 10.1103/RevModPhys.83.1245.

EADS ASTRIUM. Columbus Payload Accommodation Handbook, COL-RIBRE-MA-0007–00. *EADS Astrium*, **2**, 1–335, 2009.

Gaza, R., E.G. Yukihara, and S.W.S. McKeever. The use of optically stimulated luminescence from Al2O3:C in the dosimetry of high-energy heavy charged particle fields. *Radiat. Prot. Dosim.*, **120 (1–4)**, 354–357, 2006, DOI: 10.1093/rpd/nci574.

Guelev, M.G., I.T. Mischev, B. Burgkhardt, and E. Piesch. A two-element CaSO4:Dy dosemeter for environmental monitoring. *Radiat. Prot. Dosim.*, **51 (1)**, 35–40, 1994.

Hajek, M., T. Berger, R. Bergmann, N. Vana, Y. Uchihori, N. Yasuda, and H. Kitamura. LET dependence of thermoluminescent efficiency and peak height ratio of CaF2:Tm. *Radiat. Meas.*, **43 (2–6)**, 1135–1139, 2008, DOI: 10.1016/j.radmeas.2007.12.015.

Kodaira, S., R.V. Tolocheck, I. Ambrozova, H. Kawashima, N. Yasuda, et al. Verification of shielding effect by the water-filled materials for space radiation in the International Space Station using passive dosimeters. *Adv. Space. Res.*, **53**, 1–7, 2014, DOI: 10.1016/j.asr.2013.10.018.

Labrenz, J., S. Burmeister, T. Berger, B. Heber, and G. Reitz. Matroshka DOSTEL measurements onboard the International Space Station (ISS). *J. Space Weather Space Clim.*, **5**, A38, 2015, DOI: 10.1051/swsc/2015039.

Lishnevskii, A., M.I. Panasyuk, V.V. Benghin, V.M. Petrov, A.N. Volkov, and O.Yu. Nechaev. Variations of radiation environment on the International Space Station in 2005–2009. *Cosmic Res.*, **50 (4)**, 319–323, 2012, DOI: 10.1134/S0010952512040028.

Matthiä, D., B. Ehresmann, H. Lohf, J. Köhler, C. Zeitlin, et al. The Martian surface radiation environment – a comparison of models and MSL/RAD measurements. *J. Space Weather Space Clim.*, **6**, A13, 2016, DOI: 10.1051/swsc/2016008.

Narici, L., T. Berger, D. Matthiä, and G. Reitz. Radiation measurements performed with active detectors relevant for human space exploration. *Front. Oncol.*, **5**, 273, 2015, DOI: 10.3389/fonc.2015.00273.

NCRP Report No. 137. Fluence-based and microdosimetric event-based methods for radiation protection in space, National Council on Radiation Protection and Measurements, Bethesda, MD, 2001.

Nelson, G.A. Space radiation and human exposure, a primer. *Radiat. Res.*, **185**, 349–358, 2016, DOI: 10.1667/RR14311.1.

Pachnerová Brabcová, K., I. Ambrožová, Z. Kolísková, and A. Malušek. Uncertainties in linear energy transfer spectra measured with track-etched detectors in space. *Nucl. Instrum. Methods Phys. Res. A*, **713**, 5–10, 2013, DOI: 10.1016/j.nima.2013.03.012.

Pálfalvi, J.K. Fluence and dose of mixed space radiation by SSSNTDs: achievements and constraints. *Radiat. Meas.*, **44 (9–10)**, 724–728, 2009, DOI: 10.1016/j.radmeas.2009.10.045.

Puchalska, M., P. Bilski, T. Berger, M. Hajek, T. Horwacik, C. Körner, P. Olko, V. Shurshakov, and G. Reitz. NUNDO – a numerical model of a human torso phantom and its application to effective dose calculations for astronauts at the ISS. *Radiat. Environ. Biophys.*, **53 (4)**, 719–727, 2014, DOI: 10.1007/s00411-014-0560-7.

Reitz, G. Characteristic of the radiation field in low earth orbit and in deep space. *Z. Med. Phys.*, **18 (4)**, 233–243, 2008, DOI: 10.1016/j.zemedi.2008.06.015.

Reitz, G., R. Beaujean, C. Heilmann, J. Kopp, M. Leicher, and K. Strauch. Results of dosimetric measurements in space missions. *Adv. Space Res.*, **22 (4)**, 495–500, 1998, DOI: 10.1016/S0027-5107(99)00129-3.

Reitz, G., K. Strauch, R. Beaujean, J. Kopp, M. Luszik-Bhadra, and W. Heinrich. Dosimetric mapping inside BIORACK on shuttle missions STS76, STS81 and STS1984. In: E. Brinckmann, C. Varajão, M. Perry, Editors. *SP1222 Biorack on Spacehab*, European Space Agency, Noordwijk, Netherlands, 161–169, 1999.

Reitz, G., R. Beaujean, E. Benton, S. Burmeister, T. Dachev, S. Deme, M. Luszik-Bhadra, and P. Olko. Space radiation measurements on-board ISS – the DOSMAP experiment. *Radiat. Prot. Dosim.*, **116 (1–4)**, 374–379, 2005, DOI: 10.1093/rpd/nci262.

Reitz, G., T. Berger, P. Bilski, R. Facius, M. Hajek, et al. Astronaut's organ doses inferred from measurements in a human phantom outside the International Space Station. *Radiat. Res.*, **171 (2)**, 225–235, 2009, DOI: 10.1667/RR1559.1.

Sawakuchi, G.O., E.G. Yukihara, S.W.S. McKeever, E.R. Benton, R. Gaza, Y. Uchihori, N. Yasuda, and H. Kitamura. Relative optically stimulated luminescence and thermoluminescence efficiencies of Al2O3:C dosimeters to heavy charged particles with energies relevant to space and radiotherapy dosimetry. *J. Appl. Phys.*, **104**, 124903, 2008, DOI: 10.1063/1.3041655.

Spurny, F., and I. Jadrnickova. Dependence of thermoluminescent detectors relative response on the linear energy transfer; some examples of use. *Radiat. Meas.*, **44 (2–6)**, 944–947, 2008, DOI: 10.1016/j.radmeas.2007.11.041.

Straube, U., T. Berger, G. Reitz, F. Facius, C. Fuglesang, T. Reiter, V. Damann, and M. Tognini. Operational radiation protection for astronauts and cosmonauts and correlated activities of ESA medical operations. *Acta Astronaut.*, **66**, 963–973, 2010, DOI: 10.1016/j.actaastro.2009.10.004.

Uchihori, Y., and E.R. Benton, Editors. Results from the first two intercomparison of dosimetric instruments for cosmic radiation with heavy ions beams at NIRS (ICCHIBAN-1&2) experiments. *HIMAC Report 078*, National Institute of Radiological Sciences, Chiba, Japan, 2004.

Vanhavere, F., J.L. Genicot, D. O'Sullivan, D. Zhou, and F. Spurny. Dosimetry of biological experiments in space (DOBIES) with luminescence (OSL and TL) and track etch detectors. *Radiat. Meas.*, **43 (2–6)**, 694–697, 2008, DOI: 10.1016/j.radmeas.2007.12.002.

Warren, C.S., and W.L. Gill. Radiation dosimetry aboard the spacecraft of the eight Mercury-Atlas mission (MA-8). *NASA TN D-1862*, U.S. Govt. Printing Office, Washington, D.C., 1964.

Yasuda, N., K. Namiki, Y. Honma, Y. Umeshima, Y. Marumo, H. Ishii, and E.R. Benton. Development of a high speed imaging microscope and new software for nuclear track detector analysis. *Radiat. Meas.*, **40 (2–6)**, 311–315, 2005, DOI: 10.1016/j.radmeas.2005.02.013.

Yukihara, E.G., G.O. Sawakuchi, S. Guduru, S.W.S. McKeever, R. Gaza, E.R. Benton, N. Yasuda, Y. Uchihori, and H. Kitamura. Application of Optically Stimulated Luminescence (OSL) technique in space dosimetry. *Radiat. Meas.*, **41 (9–10)**, 1126–1135, 2006, DOI: 10.1016/j.radmeas.2006.05.027.

Zeitlin, C., D. Hassler, F. Cucinotta, B. Ehresman, R. Wimmer-Schweingruber, et al. Measurements of energetic particle radiation in transit to Mars on the Mars science laboratory. *Science*, **340**, 1080–1084, 2013, DOI: 10.1126/science.1235989.

Zhou, D., E. Semones, R. Gaza, and M. Weyland. Radiation measured with passive dosimeters in low Earth orbit. *Adv. Space Res.*, **40 (11)**, 1575–1579, 2007a, DOI: 10.1016/j.asr.2006.12.003.

Zhou, D., E. Semones, R. Gaza, S. Johnson, N. Zapp, and M. Weyland. Radiation measured for ISS-Expedition 12 with different dosimeters. *Nucl. Instrum. Methods A*, **580 (3)**, 1283–1287, 2007b, DOI: 10.1016/j.nima.2007.06.091.

Cite this article as: Berger T, Przybyla B, Matthiä D, Reitz G, Burmeister S, et al. DOSIS & DOSIS 3D: long-term dose monitoring onboard the Columbus Laboratory of the International Space Station (ISS). *J. Space Weather Space Clim.*, **6**, A39, 2016, DOI: 10.1051/swsc/2016034.